THEORETICAL AND EXPERIMENTAL INVESTIGATION OF CONDENSATION ON AMPHIPHILIC NANOSTRUCTURED SURFACES

A Thesis
Presented to
The Academic Faculty

by

David Milton Anderson

In Partial Fulfillment
of the Requirements for the Degree
Master of Science in the
School of Mechanical Engineering

Georgia Institute of Technology
May 2013

THEORETICAL AND EXPERIMENTAL INVESTIGATION OF CONDENSATION ON AMPHIPHILIC NANOSTRUCTURED SURFACES

Approved by:

Dr. Andrei G. Fedorov, Advisor
School of Mechanical Engineering
Georgia Institute of Technology

Dr. Samuel Graham
School of Mechanical Engineering
Georgia Institute of Technology

Dr. Peter A. Kottke
School of Mechanical Engineering
Georgia Institute of Technology

Dr. Mohan Srinivasarao
School of Materials Science and Engineering
Georgia Institute of Technology

Date Approved: March 5, 2013

"The ultimate measure of a man is not where he stands in moments of comfort and convenience, but where he stands at times of challenge and controversy."

- *Martin Luther King, Jr.*

ACKNOWLEDGEMENTS

It would be inappropriate to proceed without first acknowledging the contributions of numerous individuals whose influence has been critical in both the completion of this work and in my development as a researcher. I would like to start by thanking my advisor, Professor Andrei Fedorov, for being a constant source of encouragement, knowledge, support and enthusiasm. I would also like to thank many other current and former MITf lab group members for their input and support, in particular Drs. Peter Kottke and Konrad Rykaczewski. Lastly, I am grateful for the invaluable contributions of Professor Vladimir Tsukruk, Dr. Maneesh Gupta and Swati Naik of the Surface Engineering and Molecular Assemblies Laboratory at Georgia Institute of Technology and Drs. Andrey Voevodin, Chad Hunter and Shawn Putnam of the Thermal Sciences Division at Air Force Research Laboratory.

On a personal note, I would like to thank my wife Allison for always believing in me and supporting my decision to pursue graduate school. I would also like to thank my parents, Emery and Carolyn Anderson for their continued support and my good friend Dr. Taymour Hammoudi for helping give me perspective on what it means to be a scientist.

Lastly, I would like to acknowledge financial support from the U.S. Air Force Office of Scientific Research (award number FA9550-09-1-0162) and a Paper Science and Engineering Fellowship from the Georgia Tech Institute of Paper Science and Technology.

TABLE OF CONTENTS

LIST OF TABLES

LIST OF FIGURES

LIST OF SYMBOLS AND ABBREVIATIONS

a	droplet base diameter
d_{pore}	pore-to-pore spacing
f	area fraction (ratio of droplet contact area to projected area)
h	droplet height
J	droplet nucleation rate
J_o	kinetic constant of nucleation
k	Boltzmann constant
l_{wire}	nanowire length
$l_{critical}$	critical nanowire length for wetting state transition
n_{wires}	number of wires beneath droplet of base diameter a
r	roughness ratio (actual surface area to projected area)
$r_{critical}$	critical roughness ratio for wetting state transition
r_{wire}	nanowire radius
R	droplet radius of curvature
$R_{initial}$	initial droplet radius of curvature
T	absolute temperature
ΔA_{ij}	change in interfacial area between interfaces i and j
ΔG	change in Gibbs Free Energy
γ_{ij}	interfacial energy for interface of i and j
θ_a	advancing contact angle
θ_{CB}	Cassie-Baxter equilibrium contact angle
θ_r	receding contact angle

θ_W	Wenzel equilibrium contact angle
θ_Y	intrinsic (Young's) contact angle

ESEM	Environmental Scanning Electron Microscopy
PECVD	Plasma-Enhanced Chemical Vapor Deposition

SUMMARY

Condensation of water vapor is an everyday phenomenon which plays an important role in power generation schemes, desalination applications and high-heat flux cooling of power electronic devices. Continuous dropwise condensation is a desirable mode of condensation in which small, highly-spherical droplets regularly form and shed off the surface before a thick liquid is formed, thereby minimizing the thermal resistance to heat transfer across the condensate layer. While difficult to induce and sustain, dropwise condensation has been shown to achieve heat and mass transfer coefficients over an order of magnitude higher than its filmwise counterpart. Superhydrophobic surfaces have been extensively studied to promote dropwise condensation with mixed results; often surfaces that are superhydrophobic to deposited droplets formed in the gas phase above the surface do not retain this behavior with condensed droplets nucleated and grown on the surface. Recently, nanostructured superhydrophobic surfaces have been developed that are robust to vapor condensation; however, these surfaces still are not ideal for condensation heat transfer due to the high thermal resistance of the vapor layer trapped underneath the droplets and the reduced footprint of direct contact between the highly-spherical droplets and the underlying substrate.

This work has two main objectives. First, a comprehensive free energy based thermodynamic model is developed to better understand why traditional superhydrophobic surfaces often lose their properties when exposed to condensed droplets. The model is first validated using data from the existing literature and then extended to analyze the suitability of amphiphilic (*e.g.* part hydrophobic and part hydrophilic) nanostructured surfaces for condensation applications. Secondly, one of the promising amphiphilic surfaces identified by the thermodynamic model is fabricated and tested to observe condensation dynamic behavior. Two complementary visualization techniques, environmental scanning electron microscopy (ESEM) and optical (light) microscopy, are used to probe the condensation behavior and compare the performance to that of a traditional superhydrophobic surface. Observations from the condensation experiments are used to propose a new mechanism of coalescence that governs the

temporal droplet size distribution on the amphiphilic nanostructured surface and continually generates fresh sites for the droplet nucleation and growth cycle that is most efficient at heat transfer.

CHAPTER 1

INTRODUCTION

Though wettability has long been understood to depend on surface chemistry and morphology [1], intriguing opportunities to control nanostructure and create surface energy gradients with novel nanofabrication techniques have recently generated a surge of research interest in this field [2-4]. Such surfaces can produce previously unobserved modes of droplet dynamics during condensation and challenge the current understanding of physical mechanisms at multiple length scales [5] that underlie different stages of the process, especially relevant to collective droplet dynamics during growth and coalescence [6]. These new insights can be harnessed to design "smart" nanostructured surfaces which can intrinsically (*i.e.*, without external stimuli) control the dynamics of droplet nucleation, growth, and coalescence events to maximize heat and mass transfer rates. Such advances are critical for many technologies in different industries, including high performance microprocessors, high energy density batteries, and optoelectronic devices, which are becoming thermally limited and whose thermal management requires major advances in our ability to control phase-change phenomena on the nanoscale. Condensation is also a key phenomenon in numerous more-established industries, such as steam power, desalination and paper manufacturing plants.

A combined theoretical and experimental approach is taken in this thesis to investigate a specific type of "smart" surfaces – amphiphilic (*e.g.* partially hydrophobic and partially hydrophilic) nanostructure arrays - that can enhance condensation heat and mass transfer rates. After reviewing in Chapter 2 the different mechanisms by which a

liquid can interact with a rough surface and discussing the latest approaches to induce dropwise condensation using superhydrophobic surfaces, Chapter 3 develops and validates a thermodynamic free energy based model which can provide additional information about the preferred wetting state beyond what is given by the classical models. This thermodynamic model is then used to assess the potential of amphiphilic interfaces made of dense nanostructures to sustain dropwise condensation.

Recognizing that the thermodynamic model can only provide information regarding preferred equilibrium states, experimental studies are also carried out in Chapter 4 to investigate the dynamics of nucleation, growth and coalescence of droplets on an amphiphilic surface consisting of a closely packed, vertically aligned hydrophilic nanowire array with hydrophobized tips. Complementary environmental scanning electron microscopy (ESEM) and optical (light) microscopy are employed; taking advantage of enhanced spatial resolution of the former and faster frame rate and wider field of view of the latter. The condensation experiments show that droplets on the amphiphilic interface are fluidically linked by a wetted sublayer that fills the entire hydrophilic region of the surface, thereby allowing neighboring droplets to coalesce more rapidly and simultaneously in large ensembles. A mechanism for these newly observed long-range coalescence events is proposed based on fluidic communication between differently sized droplet by the Laplace pressure-driven flow through the wetted sublayer. Chapter 5 summarizes the major findings of this thesis and outlines potential areas for future work.

CHAPTER 2

SUPERHYDROPHOBIC SURFACES AND DROPWISE CONDENSATION

The manner in which a condensed liquid interacts with an underlying substrate has a considerable effect on the achievable rate of heat and mass transfer on a surface. Two distinct condensation modes are typically observed: either a continuous liquid film forms on the surface or discrete condensate droplets due to incomplete wetting of the surface. Filmwise condensation generates a growing condensate layer that restricts heat transfer due to an increase in thermal resistance with the film thickness growth. In contrast, in dropwise condensation, droplets form and are continually swept off a surface by gravity or vapor shear, allowing repetition of the nucleation and growth cycle which is most efficient for moisture/heat management [7, 8]. Both of these distinct condensation modes are illustrated in Figure 1. Indeed, although it is more difficult to achieve and sustain, dropwise condensation allows the cooled surface to be dynamically re-wetted through random droplet nucleation and growth and therefore provides heat and mass transfer coefficients over an order of magnitude higher than its filmwise counterpart [9-11]. Droplets typically leave the surface by a rolling mechanism; therefore contact line pinning and contact angle hysteresis (*e.g.* the difference between advancing and receding contact angle) must be minimized to promote easy removal of the condensate.

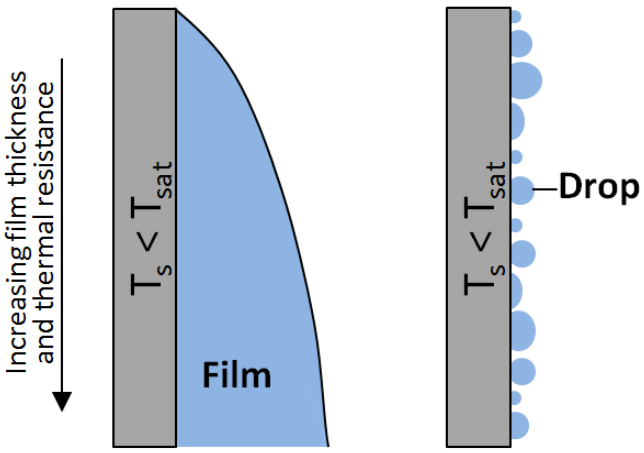

Figure 1: Filmwise vs. dropwise condensation

2.1 Wetting of Ideal Surfaces: Young's Equation

In order to quantify the expected macroscopic contact angle of a liquid droplet interacting with a real surface, it is necessary to first understand how a droplet interacts with an ideal smooth substrate of the same material. The intrinsic contact angle, θ_y, formed between a small liquid droplet and a perfectly smooth surface is calculated by Young's equation [1, 2]:

$$\cos\theta_y = \frac{\gamma_{SV} - \gamma_{SL}}{\gamma_{LV}} \tag{1}$$

where γ_{SV}, γ_{SL}, and γ_{LV} are the surface energies associated with the solid-vapor, solid-liquid and liquid-vapor interfaces, respectively. Surface energy and surface tension are often used interchangeably, as the work to create a unit of surface area is equal to the force applied per unit length. Therefore, Young's equation balances surface tension forces at the contact line and also minimizes the total surface energy of all three interfaces Figure 2a illustrates the intrinsic contact angle and the surface tension force balance at the contact line.

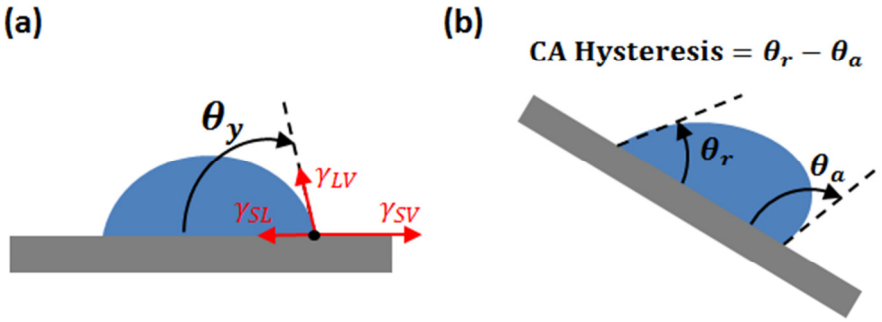

Figure 2: Young's contact angle on ideal smooth surface. (a) definition of contact angle and surface energy terms. (b) definition of contact angle (CA) hysteresis

If the substrate is tilted, as illustrated in Figure 2b, the droplet shape will deviate from a spherical cap. The advancing contact angle, θ_a, is defined as the contact angle at the leading edge of the droplet just before it starts to slide on the substrate. Similarly the receding contact angle, θ_r, is the angle formed by the droplet and the substrate at the trailing edge of the droplet as it slides. The advancing contact angle is always greater than the receding angle, and the difference between these two is defined as the contact angle hysteresis. A droplet with low contact angle hysteresis is easier to slide off a surface.

Knobler and Beysens experimentally found three distinct regimes of droplet growth during condensation on smooth silanized surfaces with intrinsic contact angle of roughly 90° [12]. In the initial stage, the surface coverage is low (less than 30% area coverage) and the growth of each isolated drop is governed by a diffusion process. Once the coverage becomes high enough for droplets to interact with one another, the mean droplet radius begins to grow more rapidly as the growth rate is enhanced by coalescences of neighboring droplets. At very large times (typically > 300s) past the

onset of condensation, a third regime exists with a bimodal droplet size distribution consisting of small droplets (which grow at a rate similar to the first regime) disbursed between a few large droplets. Eventually the large droplets become sufficiently large that gravitational forces cause them to flow off the surface.

Numerical studies [13] of 3D droplets on smooth, hydrophobic 2D surfaces showed that the mean droplet radius during the first regime (*e.g.* low surface coverage with isolated drops) scales as $\langle R \rangle \propto t^{1/3}$, a result that was consistent with the previously mentioned experimental observations [12]. In the second regime, both experiments and simulations by Knobler *et al.* and Meakin *et al.* found the droplet radius to scale according to $\langle R \rangle \propto t^{1}$, with the higher growth rate being due to interactions between adjacent droplets occurring with high surface coverage [12, 14-16].

2.2 Surface Models of Wetting for Rough Surfaces

All real surfaces possess some degree of roughness, which tends to enhance their natural wetting properties, making mildly hydrophobic surfaces more hydrophobic and conversely mildly hydrophilic surfaces more hydrophilic. The manner in which a liquid droplet interacts with a rough hydrophobic surface can broadly be classified into either the Wenzel or the Cassie-Baxter state.

The Wenzel state occurs when a liquid droplet fully penetrates the rough features on a surface, thereby increasing the amount of solid-liquid interfacial area over what would be experienced by a droplet with the same base area on a smooth surface. The Wenzel state is also sometimes referred to as “homogeneous” wetting because the resulting interface consists only of liquid-solid contact. Alternatively the Cassie-Baxter state, in which the liquid droplet rests on top of the roughness features, traps air within

the grooves and forms a composite "heterogeneous" interface of liquid-solid and liquid-gas beneath the droplet. The two primary wetting states are illustrated in Figure 3.

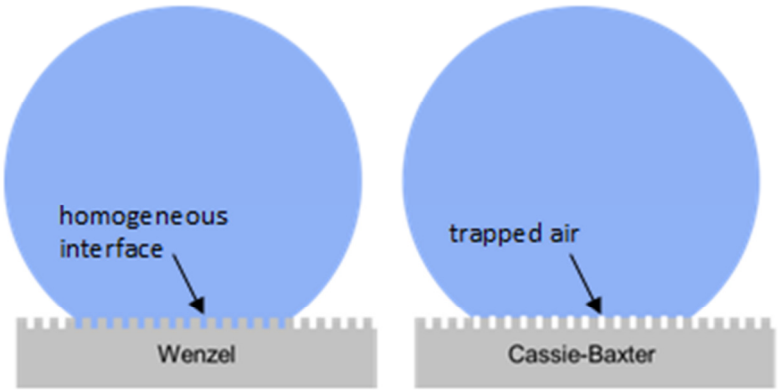

Figure 3: Liquid droplet in Wenzel vs. Cassie-Baxter wetting state

So-called "Cassie" droplets are substantially more mobile than their Wenzel counterparts, where the liquid that has penetrated the roughness features causes contact line pinning [17, 18]. This distinction between Cassie and Wenzel droplets is important in understanding the "superhydrophobic" behavior of certain surfaces. To be considered superhydrophobic, a surface must exhibit both a water contact angle greater than 150° and contact angle hysteresis less than 5° [3]. A surface that interacts with water in the Wenzel state, although it may demonstrate a high contact angle, is not truly superhydrophobic because it will exhibit significant contact angle hysteresis caused by pinning of the contact line. Only the Cassie-Baxter state allows droplets to freely roll off the surface; hence, the extensive body of dropwise condensation research has focused on superhydrophobic surfaces and the associated rolling mechanism [19-25]. The highest possible water contact angle for hydrophobic smooth surfaces is approximately 115° [2];

therefore some degree of roughness is required to amplify the hydrophobic nature of a material and make it truly superhydrophobic.

Proposed in 1936, the Wenzel model [26] was the first method developed to calculate the theoretical macroscopic contact angle formed between a liquid droplet and a rough surface. In the case of the liquid droplet fully penetrating the roughness features on a solid, Wenzel derived the apparent contact angle to be:

$$\cos\theta_W = r\cos\theta_y \tag{2}$$

where θ_w is the apparent macroscopic contact angle. The roughness factor, r, modifies the intrinsic contact angle θ_y and is defined by:

$$r = \frac{actual\ surface\ area}{planar\ area\ beneath\ droplet} \tag{3}$$

Note that for a perfectly smooth surface, $r = 1$ and Young's equation is recovered. For any real surface with some degree of roughness, r will always be greater than unity. The Wenzel model performs well for surfaces with moderate roughness; however, it is clear that for an intrinsically hydrophobic surface ($\theta_y > 90^o$), if the roughness factor is large enough, the cosine of the contact angle as defined by equation (2) will exceed -1. This result is mathematically impossible, indicating that another model is required to describe the wetting behavior on this type of surface.

The Cassie-Baxter model [27], developed in 1944, considers an alternate scenario in which air pockets are trapped underneath a droplet, and the energetic contributions of both the solid-liquid interface and liquid-air interface beneath the droplet must be considered. Cassie and Baxter derived the relation for the apparent contact angle, θ_{CB}, of a droplet resting on a heterogeneous interface:

$$\cos\theta_{CB} = f\cos\theta_y + f - 1 \quad (4)$$

In the Cassie-Baxter model, the area fraction, *f*, is the key geometric parameter that modifies Young's contact angle and determines the macroscopic contact angle. The area fraction, always less than unity, is defined as:

$$f = \frac{surface\ \ area\ wetted\ by\ water}{planar\ surface\ area\ below\ the\ droplet} \quad (5)$$

Again, for the special case of a smooth surface, $f = 1$ and Young's equation is recovered.

One limitation of these models is that they only predict an equilibrium angle assuming the wetting occurs either solely in the Wenzel or Cassie-Baxter mode, and do not provide a quantitative assessment of which is thermodynamically favorable. Chapter 3 aims to address this issue by developing a comprehensive thermodynamic model which compares the surface energy for each wetting mode and identifies a transition between the states.

While the Wenzel and Cassie-Baxter equations have become widely accepted among surface scientists, there has been some discussion and disagreement over their validity. In 2007, Gao and McCarthy [28] proposed that the contact angle behavior is determined by interactions at the three-phase contact line alone and that the area-based arguments used by Wenzel and Cassie to derive their models are unsuitable. The claim was supported through experimental observation of composite surfaces that contain "spots" in a surrounding field: a hydrophilic spot in a hydrophobic field, a rough spot in a smooth field, and a smooth spot in a rough field. The results indicated the spots (no matter how rough/smooth or hydrophobic/hydrophilic) trapped in the three-phase contact line have no impact on the apparent contact angle [28, 29].

In response to this study, a dialogue emerged that focused on the range of applicability of the original Wenzel and Cassie-Baxter models. McHale [30] pointed out that Gao and McCarthy's experimental results were fundamentally local and restricted only to the position where the droplets sat. On the other hand, the Wenzel and Cassie-Baxter models were derived assuming, and therefore only applicable for, a surface that is everywhere similar and isotropic, rather than a "trapped spot" structure. Nosonovsky [31] also argued that the Wenzel and Cassie equations could be modified to involve local heterogeneity for surfaces such as the ones tested by Gao and McCarthy. Panchagula and Vedantam [32] similarly claimed the importance of the behavior in the vicinity of the three-phase contact line and suggested that, for "spotted" surfaces the area fraction, f, must be calculated locally near the contact line to obtain meaningful results. The surfaces considered in this thesis have roughness features and changes in the surface energy which are global (*i.e.,* uniformly distributed over the entire surface) rather than a localized "trapped spot" structure, and therefore the original Wenzel and Cassie-Baxter area-based thermodynamic energy models should remain valid.

2.3 Applications and Limitations

Superhydrophobic surfaces have broad range of potential applications. Their self-cleaning nature can be used to defog and remove debris from surfaces that need to remain optically transparent, such as vehicle windshields and instrument gauges. Additionally superhydrophobic surfaces can be used to limit bacterial adhesion/growth and for oil-water separation purposes [4]. Many potential applications involve nucleation and water vapor condensation, as this is an everyday phenomenon which plays an important role in the formation of dew, phase-change heat transfer, steam nucleation in power turbines,

aerosol detection, water recovery, *etc*. Improvements in this area could lead to more efficient condensers in power generation and desalination, reduced moisture-induced efficiency losses in steam turbines, and development of high-performance heat pipes for electronics cooling applications [33].

A widely recognized challenge with superhydrophobic surfaces, as observed in nature on the Lotus leaf [34, 35] and on synthetic surfaces [36, 37], is that they are often rendered ineffective during condensation because the Wenzel state is typically at a lower interfacial free energy than the Cassie-Baxter state [38-40]. As a result, though some metastable Cassie droplets may form on the surface, eventually droplets condensed from the surrounding vapor phase will revert to the pinned Wenzel state. This is in contrast to deposited droplets that are of a diameter larger than the roughness feature spacing, and are thus able to trap air beneath them and assume the meta-stable Cassie-Baxter state [32].

On traditional superhydrophobic surface, possessing uniform low surface energy, condensate droplets will nucleate randomly on the surface at all depths within the roughness structure (tops, side walls, and valleys), preventing air from being trapped and allowing coalesced drops to form in the lower energy Wenzel state. The lack of spatial preference for condensation on a rough chemically homogeneous surface can be understood through Volmer's classical nucleation theory [23], which states that the free energy barrier ΔG for the formation of a liquid nucleus on a flat surface depends strongly on the intrinsic wettability of the surface via the intrinsic contact angle θ_y. The intrinsic wettability of the surface has a strong effect on the nucleation rate J via the inverse exponential dependence on free energy of nucleation ΔG:

$$J = J_0 \exp(-\Delta G/kT) = J_0 \exp[\pi\gamma_{LV} r^{*2}(2 - 3\cos\theta_y + \cos^3\theta_y)/3kT] \quad (6)$$

where J_0 is a kinetic constant, r^* is the critical radius of nucleation, k is the Boltzmann constant and T is absolute temperature. Therefore, a surface with uniform intrinsic wettability will be characterized by a uniform ΔG and J, and as a result heterogeneous nucleation on such surfaces occurs randomly without any particular spatial preference.

More recently, some superhydrophobic surfaces with nanoscale roughness have been demonstrated to retain their properties even during condensation [19-21, 41-43]. Lau *et al.* [19] fabricated a nanowire surface so rough that the Cassie-Baxter state was more energetically favorable than the Wenzel state and was therefore robust to condensation, but this required a sparse feature spacing (area fraction f of 0.11) combined with an aspect ratio (length/diameter) of over four, making this type of surface more difficult to fabricate and more susceptible to abrasion damage. Additionally, Miljkovic *et al.* [42] demonstrated that the Cassie-Baxter state can be actually be detrimental to heat transfer for features with too high of an aspect ratio because the conduction resistance caused by the vapor barrier underneath the droplet can outweigh the benefits of rapid droplet shedding from the surface. Further challenging the conventional wisdom that Cassie droplets are the best for dropwise condensation, the recent work of Rykaczewski *et al.* [44] showed that during the initial growth of sub-10 μm droplets, a lower contact angle is beneficial to heat transfer because the larger base area decreases the conduction heat transfer resistance from the underlying substrate. Lower contact angles are typically associated with Wenzel droplets, hence a surface that could effectively regenerate nucleation sites for droplets in the Wenzel mode might be much more ideal for dropwise condensation heat transfer than one with high contact angle Cassie droplets.

2.4 Summary

This chapter reviewed the different modes in which a liquid droplet can interact with an underlying substrate and discussed the implications on condensation heat and mass transfer. Generally speaking, an ideal condensing surface should possess the following characteristics:

1) It creates a large contact area between the liquid and the underlying substrate;
2) It possesses a low free energy barrier for nucleation (associated with hydrophilicity);
3) It provides a mechanism for easy liquid removal from the surface prior to the condensate layer becoming thick enough to become a barrier to significantly restrict heat transfer across the liquid film; and
4) It enables an efficient surface re-wetting upon removal of the previously formed condensate.

Traditional superhydrophobic surfaces typically struggle to fully meet all four of the above stated requirements because condensate tends to form in the sticky Wenzel state with fairly large apparent contact angle (small contact surface area). Even if the "stickiness" of the superhydrophobic surfaces is managed with nanoscale architectures to be robust to condensation, such surface have an intrinsically large kinetic energy barrier for droplet nucleation and cannot be uniformly re-wetted. Because of these limitations, the remaining chapters of this thesis investigate amphiphilic surfaces which have a potential of circumnavigating at least some of the challenges associated with the use of the conventional superhydrophobic surfaces for the effective moisture management in condensation.

CHAPTER 3

FREE ENERGY WETTING ANALYSIS

As outlined in Chapter 2, traditional superhydrophobic surfaces often lose their effectiveness when wetted by condensation, tending to form sticky Wenzel droplets with a high degree of contact angle hysteresis as opposed to mobile Cassie droplets. In order to better understand this behavior, this chapter develops a thermodynamic model to calculate the free energy of a droplet resting on a rough hydrophobic surface as a function of its macroscopic contact angle and its mode of interaction with the solid (*e.g.* Wenzel *vs.* Cassie-Baxter state). The contact angle for each wetting mode with the lowest surface energy corresponds to that mode's equilibrium contact angle, and a comparison of the relative free energy between the equilibrium Wenzel and Cassie-Baxter states allows one to identify which of these wetting modes is a global versus only a local energy minimum.

3.1 Modeling Approach and Assumptions

A liquid droplet deposited on a rough hydrophobic surface can be viewed as a closed thermodynamic system that includes only the liquid and its surface interactions. The initial and final state of this system are illustrated in Figure 4. In the initial (reference) state, the droplet has not yet touched the surface and assumes a perfectly spherical shape. Once the droplet contacts and begins to interact with the surface, the contact angle is initially 180° but the droplet will deform until the system reaches a new free energy minimum. The radius of curvature also must change from its initial value to satisfy mass conservation.

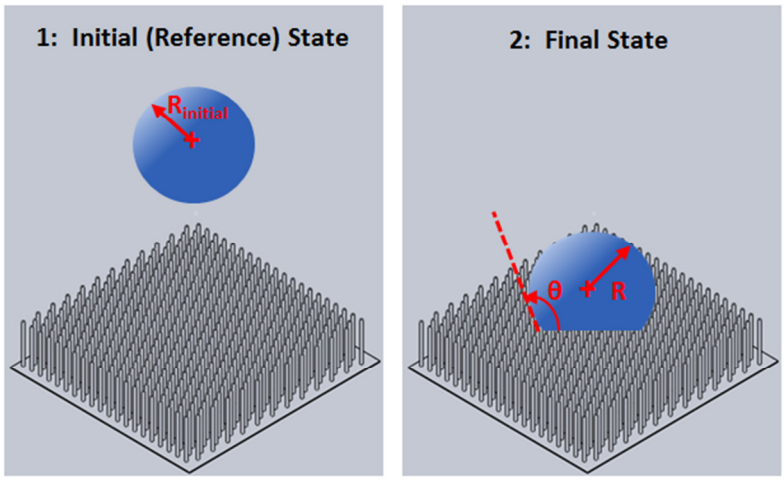

Figure 4: Initial and final states for thermodynamic free energy model

In modeling the free energy of the droplet, it is assumed that surface energy is the dominant contributor to the overall change in free energy between the initial and final states. The droplets studied in this thesis are smaller than the capillary length scale, or the droplet size above which gravity forces begin to deform droplets from a perfectly spherical shape, allowing neglection of gravitational potential energy terms. Also it is assumed the kinetic energy associated with the droplet velocity in the initial state is negligible (*e.g.* it is gently deposited on the surface). Lastly, the fluid is assumed to be incompressible such that any change in internal Laplace pressure does no significant boundary work.

With those simplifying assumptions in place, the change in free energy between the initial and final state as a function of contact angle can be expressed only as the product of interfacial energy and the change in area of each interface summed over all the different interfaces:

$$\Delta G(\theta) = \sum \gamma_{ij} \cdot \Delta A_{ij}(\theta) \tag{7}$$

In the above equation, *ij* can take one of three values depending on the type of interface: solid-liquid (SL), solid-vapor (SV) or liquid-vapor (LV). In order to calculate the change in area of each interface as a function of the macroscopic contact angle, $\Delta A_{ij}(\theta)$, it is necessary to define relevant geometric parameters pertaining to the surface. For consistency, the free energy model utilizes the roughness factor, *r*, and area fraction, *f*, as outlined for the Wenzel and Cassie-Baxter wetting modes in equations (3) and (5), respectively. The hydrophobic surface under consideration is a staggered packed configuration of uniform diameter and height nanowires. An overhead view of this geometry is shown in Figure 5.

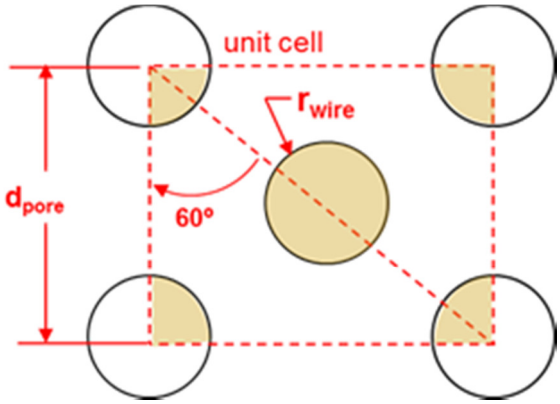

Figure 5: Overhead view of nanowire post array. Dimensions of repeating unit cell are used to calculate roughness factor, *r*, and area fraction, *f*.

Although a practically realized nanowire array typically will have some small variation in height amongst the wires, the model assumes that the wires all are of uniform height l_{wire}. Using this assumption, the roughness factor and area fraction can be calculated for this surface:

$$r = 1 + \frac{4\pi}{\sqrt{3}} \cdot \frac{r_{wire} \times l_{wire}}{(d_{pore})^2} \tag{8}$$

$$f = \frac{2\pi}{\sqrt{3}} \left[\frac{r_{wire}}{d_{pore}}\right]^2 \tag{9}$$

With *r* and *f* defined, it is possible to calculate the change in area of each type of interface (solid-liquid, solid-vapor, and vapor-liquid) as a function of the macroscopic contact angle. Equation (7) can then be used to calculate the change in free energy between the initial and final state to determine the thermodynamically preferred contact angle.

3.2 Model Development

Because the droplet fully penetrates the roughness features in the Wenzel mode but rests on the feature tops in the Cassie-Baxter mode, it is obvious that the change in area for each type of interface from the initial reference state to the final state in Figure 4 will depend on which wetting mode the droplet adopts. It is assumed that the droplet only interacts with the surface in one of the two modes, *i.e.* no partial Wenzel/Cassie-Baxter behavior occurs.

In the Wenzel state, the droplet fully penetrates the surface roughness features, as illustrated in Figure 6.

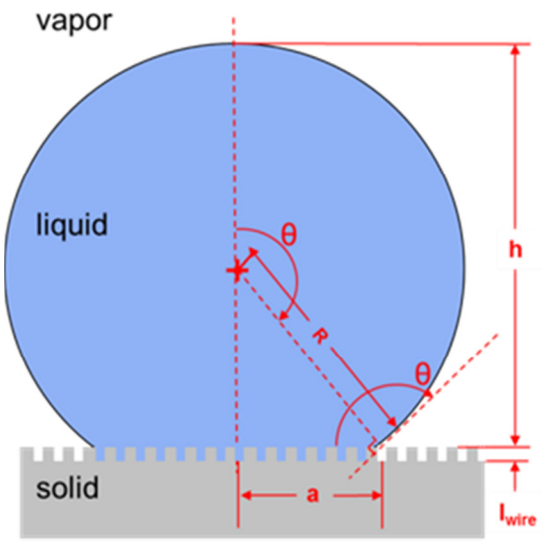

Figure 6: Wenzel state droplet geometric relations used to calculate the change in area of each interface from the initial (reference) to a given thermodynamic state

The base radius (a), droplet height (h), and radius of curvature (R) can be related to the macro-scale apparent contact angle (θ) by the following geometric relations:

$$a = Rsin\theta \tag{10}$$

$$h = R(1 - cos\theta) \tag{11}$$

Additionally, a volume conservation relation, valid because the droplet is an incompressible fluid, provides the final constraint required to solve for a, h, and R as a function of macroscopic contact angle θ:

$$\frac{4}{3}\pi R_{initial}^3 = \frac{\pi h}{6}[3a^2 + h^2] + (1 - f)(\pi a^2)l_{wire} \tag{12}$$

The second term on the right side of equation (12) represents the fluid volume trapped between the roughness features and is typically (for microscale droplets on nanoscale roughness features) many orders of magnitude smaller than the volume of the portion of the droplet above the surface, leading to an approximation:

$$\frac{4}{3}\pi R_{initial}^3 \cong \frac{\pi h}{6}[3a^2 + h^2] \tag{13}$$

The change in interfacial areas from the reference state for a Wenzel (W) drop can be expressed using geometric relations:

$$\Delta A_{LV,W} = 2\pi Rh - 4\pi R_{initial}^2 \tag{14}$$

$$\Delta A_{LS,W} = \pi a^2 + n_{wires} \cdot 2\pi r_{wire} \cdot l_{wire} \tag{15}$$

$$\Delta A_{SV,W} = -\Delta A_{LS,W} \tag{16}$$

with the number of wires underneath the base of the droplet calculated by:

$$n_{wires} = f \left\lfloor \frac{a}{r_{wire}} \right\rfloor^2 \tag{17}$$

In order for equations (13) and (17) to be valid, the droplet must be significantly larger than the roughness length scale such the liquid volume within and contact line curvature around individual features can be neglected. To enhance condensation heat transfer rates, droplets with diameters on the order of 10-100 μm must be removed from the surface before they become large enough for conduction resistance across the water layer to restrict heat transfer [7]; therefore, the droplets considered in this thesis are several orders of magnitude larger than nanoscale roughness features and the model assumption is appropriate.

Finally, the change in free energy for the Wenzel state is the sum of the change in surface area of each interface from the reference state multiplied by its respective interfacial energy:

$$\Delta G_W = \gamma_{LV}\Delta A_{LV,W} + (\gamma_{LS} - \gamma_{SV})\Delta A_{LS,W} \tag{18}$$

As opposed to forming a homogeneous liquid-solid interface, it is also possible for the droplet deposited on the surface to assume the Cassie-Baxter state, as illustrated in Figure 7. Because the liquid volume between the grooves in the Wenzel state is

insignificant compared to the volume of the spherical cap above the surface, the Wenzel state's volume conservation equation (13) is also valid for the Cassie-Baxter model.

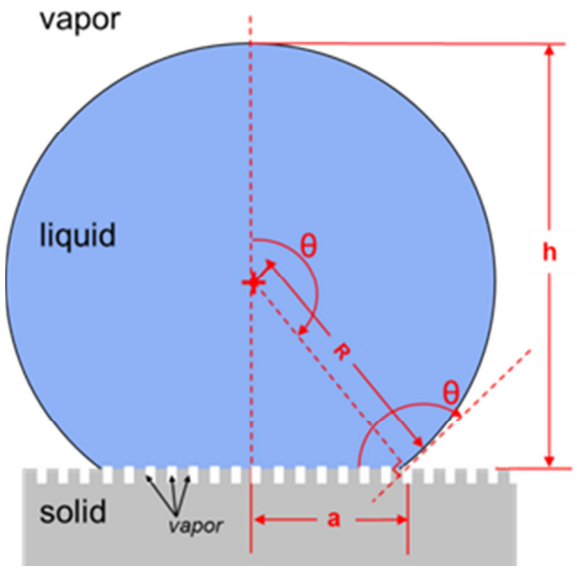

Figure 7: Cassie-Baxter state droplet geometric relations used to calculate the change in area of each interface from the initial (reference) to a given thermodynamic state

The Wenzel equations (10) and (11) for the base radius (a) and droplet height (h) also apply to the Cassie-Baxter configuration. The change in area for each type of interface from the reference to the Cassie-Baxter (CB) state is expressed with the following equations:

$$\Delta A_{LV,CB} = 2\pi Rh + \pi a^2(1-f) - 4\pi R_{initial}^2 \tag{19}$$

$$\Delta A_{LS,CB} = [\pi a^2]f \tag{20}$$

$$\Delta A_{SV,CB} = -\Delta A_{LS,CB} \tag{21}$$

Giving the overall change in free energy of a droplet in the Cassie-Baxter state as:

$$\Delta G_{CB} = \gamma_{LV}\Delta A_{LV,CB} + (\gamma_{LS} - \gamma_{SV})\Delta A_{LS,CB} \tag{22}$$

Equations (18) and (22) are used, in combination with the appropriate relations for interfacial area changes, to determine the free energy as a function of contact angle for the Wenzel and Cassie-Baxter states, respectively.

3.3 Model Validation and Analysis

The first test applied to the free energy model developed in the previous section is whether it can predict the same contact angle as the classical Wenzel and Cassie-Baxter equations. The wire diameter and spacing are chosen to match that of Lau et al.'s study [19] to facilitate further comparisons later on. The geometric and surface energy parameters used in the model are summarized in Table 1.

Table 1: Parameters for Surface Energy Model Validation

$R_{initial}$	50 [μm]
r_{wire}	25 [nm]
d_{pore}	145 [nm]
l_{wire}	200 [nm]
r	2.7 [-]
f	0.11 [-]
γ_{LV}	72.8 [mJ/m^2]
γ_{SV}	18 [mJ/m^2]
θ_y	108°
γ_{SL}	40.5 [mJ/m^2]

Using the roughness ratio r and area fraction f, the Wenzel and Cassie-Baxter equations predict macroscopic contact angles of $\theta_W = 146.5°$ and $\theta_{CB} = 157.7°$, respectively. Figure 8 shows that the model predicts contact angles which perfectly match

the Wenzel and Cassie-Baxter results. The predictions in Figure 8 are for a 50 μm radius droplet, but if the droplet size is increased the same equilibrium angles are found, only the magnitude of the ΔG changes (not shown). This is to be expected because the Wenzel and Cassie-Baxter equations are independent of droplet size, fully consistent with the model predictions.

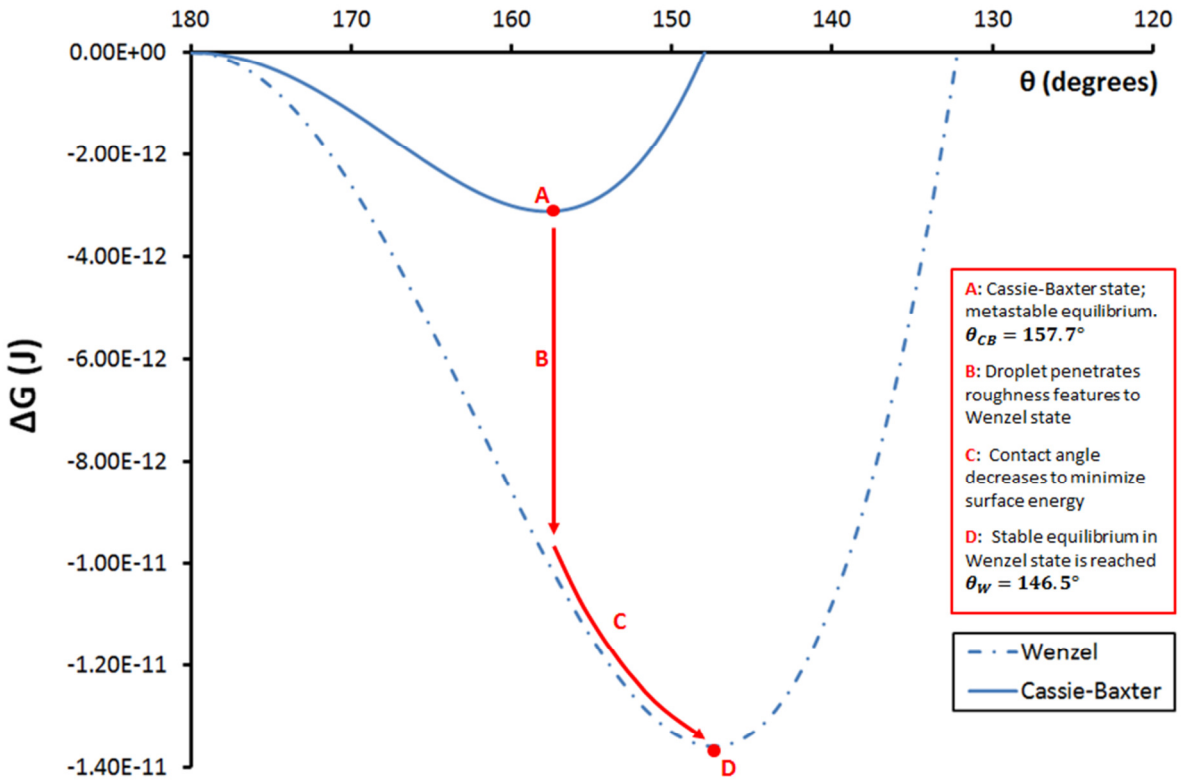

Figure 8: Predictions of free energy versus contact angle. The model predicts macroscopic contact angles equal to Wenzel and Cassie-Baxter wetting equations. The Cassie-Baxter state is metastable because it is at a higher relative energy, and A-D shows how a droplet could transition to the globally stable Wenzel state if it penetrates the roughness features.

The roughness factor r varies with the length of the wires, so it is useful to consider cases where this parameter varies. A droplet in the Cassie-Baxter state only interacts with the top of the roughness features, therefore the predicted Cassie-Baxter angle is independent of wire length. On the other hand, the Wenzel contact angle is a strong function of wire length. Therefore, along with the previous case where the wire length was such that $\theta_{CB} > \theta_W$, two additional scenarios are considered to represent cases where the predicted Wenzel contact angle is greater than or exactly equal to the Cassie-Baxter angle. The macroscopic contact angles for each wire length considered, as predicted by the Wenzel and Cassie-Baxter equations, are summarized in Table 2.

Table 2: Contact Angle Predictions Using Wenzel and Cassie-Baxter Equations for Different Nanowire Array Lengths

Macroscopic Contact Angle			
l_{wire} [nm]	r [-]	θw	θ_{CB}
200	2.70	146.5°	157.7°
231	3.00	157.7°	
250	3.16	167.3°	

Figure 9 shows the change in free energy of the droplet from the reference state as a function of macroscopic contact angle for the three different wire length cases, as computed by the thermodynamic model. In all three cases, the macroscopic contact angle corresponding to the minimum predicted surface energy by the model do match the values reported in Table 2 as computed using the Wenzel and Cassie-Baxter equations.

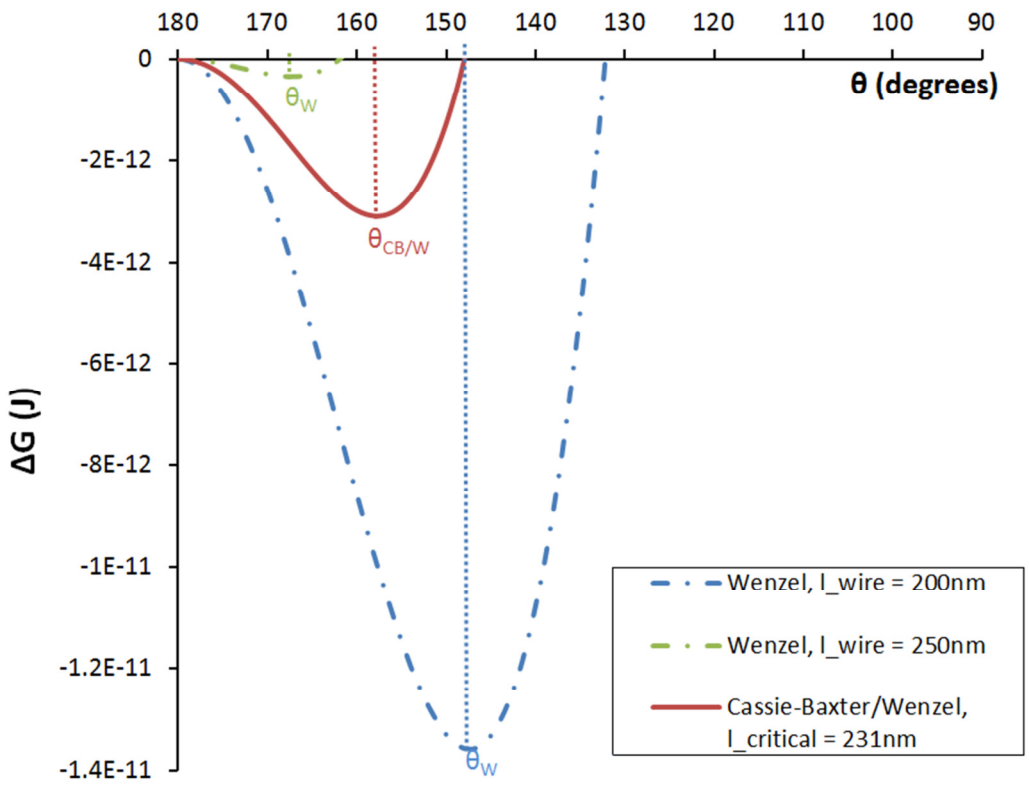

Figure 9: Change in free energy vs. contact angle for three different wire length scenarios. A wire length less than the critical length will result in the Wenzel state being at a global free energy minimum, while the Cassie-Baxter state is the global minimum for wires greater than the critical length. The Cassie-Baxter and Wenzel states have equal free energy for all values of θ if the wire is equal to the critical length.

The model does provide additional insight over just the classical Wenzel and Cassie-Baxter equations, however, by quantifying the relative difference in free energy between each state. For shorter (200nm) wires, the Wenzel state has a lower free energy in addition to a lower equilibrium contact angle, while the reverse holds true for the longer (250 nm) wires. There is a transition point, $l_{critical}$, at which not only are the equilibrium macroscopic Wenzel and Cassie-Baxter contact angles equal, but the relative free energy is equal as well. Furthermore, this equal free energy condition holds true not only at the equilibrium contact angle, but for all possible contact angles; *i.e.*, the energy

curves for both states fully overlap. For the geometry in Figure 9, this transition length occurs at $l_{critical}$ = 231 nm. In general, the critical length can be solved for by solving for a critical roughness factor, $r_{critical}$ using:

$$r_{critical} = f + \frac{f - 1}{\cos \theta_y} \tag{23}$$

which is derived by setting θ_W and θ_{CB} from equations (2) and (4) equal to one another and solving for the roughness factor.

A second validity check is applied to the surface energy model by comparing with the experimental results of Lau et al. [19]. This study reports on condensation of droplets in the Cassie-Baxter (CB) state on 50 nm diameter wires with an area fraction *f* of 0.11. In order to generate mobile (CB) droplets, the wires had to be greater than 200 nm in length, and the transition from the Wenzel state at shorter wire length to the Cassie-Baxter state was inferred by measuring dramatically lower contact angle hysteresis on the surface with longer wires. According to the free energy model, this transition of preferred energy state should occur when the equilibrium Wenzel angle exceeds that of the Cassie-Baxter state.

Figure 10 shows that the free energy model predicts a transition occurring at $l_{critical}$ = 231 nm, as close as could be expected to the experimental value given the small number of wire lengths tested. The dotted green and red lines in Figure 10 show the model predicted Wenzel and Cassie-Baxter angles for the given wire length in regions where that particular state is not energetically preferred. The surface energy model cannot predict hysteresis, as this is a local contact line phenomenon, so it is expected that the model predicted equilibrium angles are bounded at the top by the experimental advancing angle data and at the bottom by the experimental receding angle data.

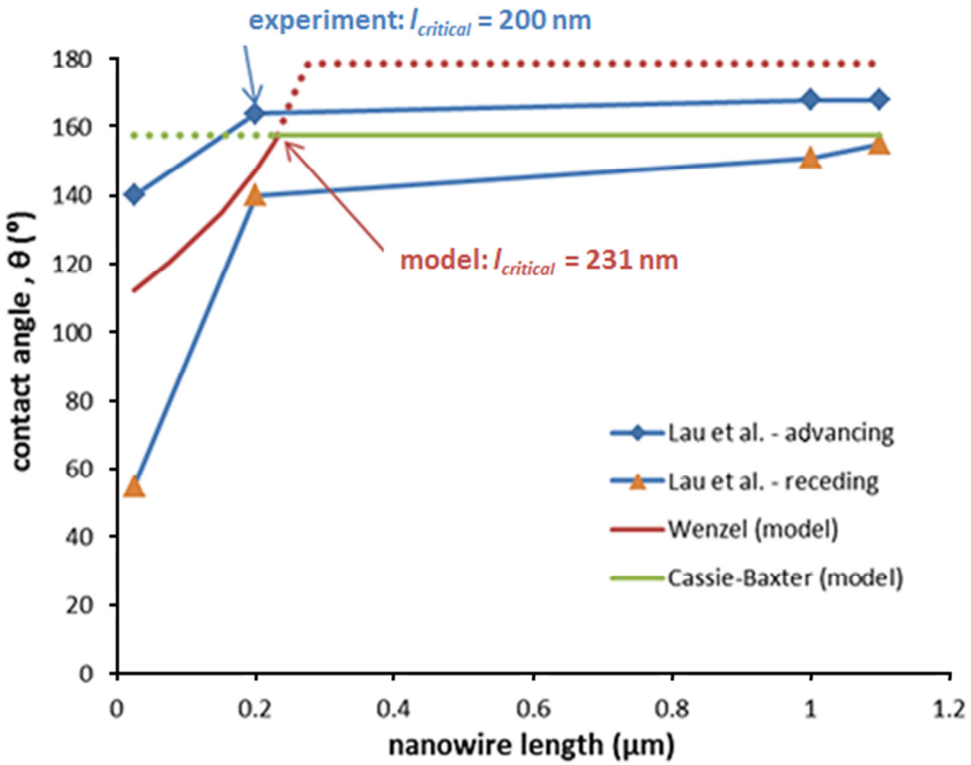

Figure 10: Condensed droplet contact angle vs. nanowire length. The transition from Wenzel to Cassie-Baxter state, as experimentally observed by a dramatic reduction in contact angle hysteresis [19] and theoretically predicted by the developed thermodynamic model as the global minimum free energy state, occurring at similar wire lengths.

The free energy model's ability to quantify the relative free energy of a droplet in the Wenzel *vs.* Cassie-Baxter state helps explain the loss of superhydrophobic properties during condensation which was outlined in Chapter 2. When droplets are free to nucleate anywhere on the surface they naturally end up in the global free energy minimum, which for moderately rough surfaces is the Wenzel state. This results in high contact angle hysteresis and the loss of the lotus effect. For surfaces above the critical roughness, the Cassie-Baxter state is observed even in condensation, but such a surface is undesirable

because its high aspect ratio will create a larger vapor barrier to heat transfer underneath the droplet, in addition to being harder to fabricate and more susceptible to damage.

3.4 Theoretical Assessment of Amphiphilic Surfaces

Having built confidence in the thermodynamic free energy model, it can be used to evaluate different geometries as well as expanded for scenarios where varying regions of the surface have different surface energies. The latter is a case where the model can calculate the expected wetting behavior while the traditional Wenzel and Cassie-Baxter equations are not able to predict the contact angle because both require a chemically homogeneous surface.

One idea that has been proposed to avoid this deficiency in condensation on traditional superhydrophobic surfaces is to make the tips of roughness features have higher surface energy (or less hydrophobic) than the rest of the surface. As suggested by equation (6), the nucleation energy barrier continuously increases with intrinsic contact angle, indicating that hydrophobic surfaces have a higher free energy barrier to nucleation when compared to hydrophilic surfaces under identical conditions. By creating specific regions on a rough surface that are more hydrophilic, it is possible to cause preferential nucleation in those locations. Experiments on condensation of water vapor on a surface with alternating hydrophobic and hydrophilic segments have verified this concept [23].

Although introducing mild hydrophilicity in targeted areas of a surface can be used to induce condensation in the desired wetting state, there is clearly a tradeoff in that doing so also will reduce the equilibrium contact angle below what it would have been if the surface were uniformly hydrophobic. Assessing this tradeoff can be done using the

free energy model, developed and validated in the previous sections, which allows for calculation of the macroscopic angle resulting in the minimum surface energy even for a surface with non-uniform surface energies.

The model developed in Section 3.2 is slightly modified to assign different values of γ_{LS} and γ_{SV} to the top and the side walls/bottom of the nanowire array. The surface energies assigned to the top of the roughness features correspond to a mildly hydrophilic θ_y of 85°. The length of the nanowires is also reduced to 100 nm, such that the thermally resistant vapor gap is cut in half. Aside from two different sets of surface energy and the wire length, the other model inputs are identical to those listed in Table 1.

Figure 11 illustrates that the expected Cassie-Baxter contact angle will reduce from $\theta_{CB} = 158°$ for a uniformly hydrophobic surface to $\theta_{CB} = 152°$ in the case of a nanorough surface with mildly hydrophilic tips. The free energy of the droplet in the Wenzel state is still a global minimum compared to that of the Cassie-Baxter state, however it is expected that condensed droplets will form in the meta-stable Cassie-Baxter regime on the hybrid surface if one were to perform a local thermodynamic analysis in the vicinity of each nanowire tops. When droplets nucleate (and are of a similar order of magnitude to the roughness features), they will naturally stay on the hydrophilic wire tops, and as they grow/coalesce to span many wires there will be air trapped beneath to provide a kinetic barrier to the larger droplet from penetrating to the Wenzel state. Conversely, surface with a uniform hydrophobicity would be expected to produce Wenzel droplets, the thermodynamically preferred state, during condensation due to spatially uniform nucleation.

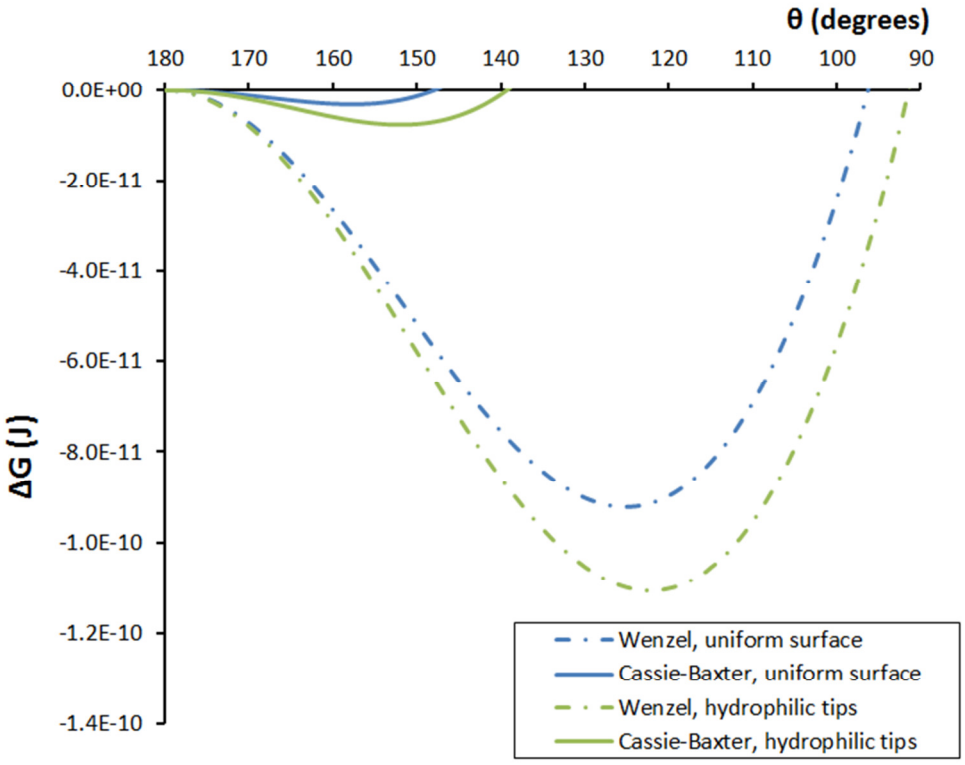

Figure 11: Free energy versus droplet contact angle for composite surface (green) and uniformly hydrophobic surface (blue). For both surfaces the Wenzel state is the global energy minimum; however, the composite surface is expected to nucleate droplets on the top of the surface, allowing condensed droplets to form in the metastable Cassie-Baxter state.

In the case of only mildly hydrophilic (θ_y = 85°) nanowire tops, the equilibrium contact angle is reduced from the uniformly hydrophobic case yet it remains above 150°, the typical threshold for a surface to be considered superhydrophobic. Figure 12 highlights the impact of increasing the hydrophilicity of the top region of the nanowires. For intrinsic contact angles less than 75°, the macroscopic Cassie-Baxter contact angle drops below the 150° threshold, and begins approaching 140° at extremely hydrophilic values for the tip surface energy. The inverse dependence of macroscopic contact angle

on the degree of nanowire tip hydrophilicity will become more severe with an increasing area fraction *f*.

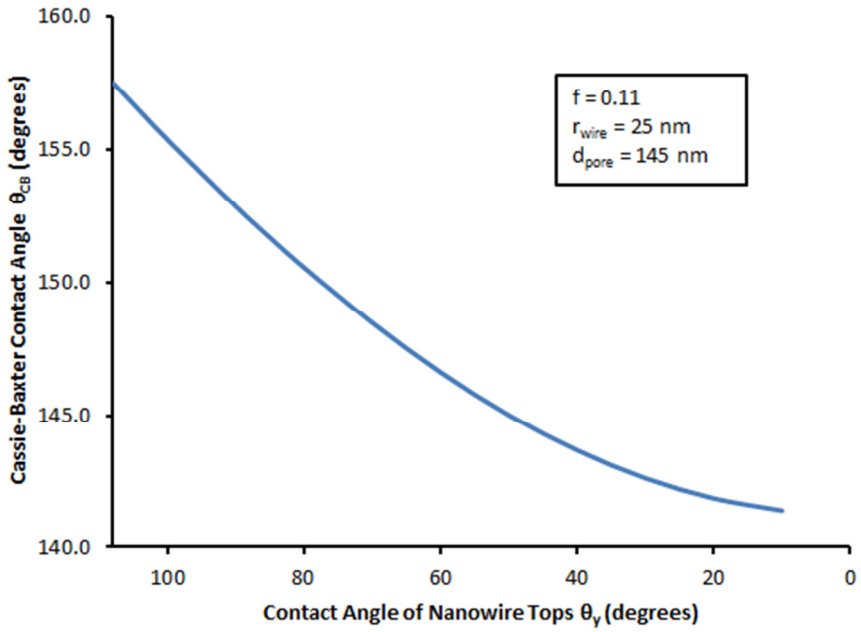

Figure 12: Cassie-Baxter contact angle reduction with decreasing intrinsic contact angle of nanowire tops. Intrinsic contact angle less than 75° reduces the contact angle below the 150° threshold for superhydrophobicity.

Though most attempts to design dropwise condensation surfaces have utilized either uniformly hydrophobic surfaces, or in the case of non-uniform surface energy a radial gradient [45] or hydrophilic tips on hydrophobic base features [23], it is possible that other energetic arrangements can induce interesting behavior that is beneficial to condensation heat transfer. To that end, the free energy model is employed to investigate thermodynamic behavior of an amphiphilic surface, depicted in Figure 13, consisting of nanowire features with hydrophobic tops on a hydrophilic base. When the surface is cooled from below, preferential nucleation is expected to occur in the hydrophilic base

region (Figure 13a) due lower free energy barrier for nucleation and a higher degree of subcooling caused by the vertical temperature gradient. The model can then predict the equilibrium contact angle corresponding to minimum free energy of a droplet by comparing the energies of the initial (reference) and final states shown in Figure 13c.

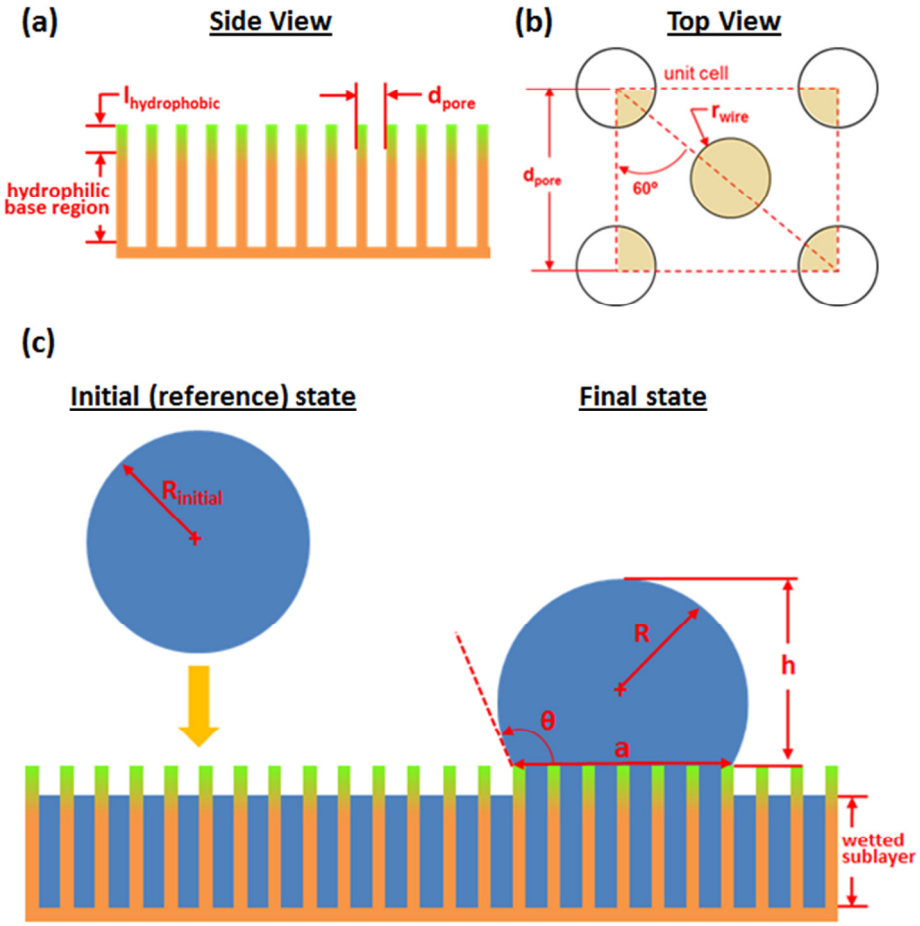

Figure 13: Amphiphilic surface consisting of a nanowire array with hydrophilic base region and hydrophobic tips. (a) Side and (b) top view used to define geometry. (c) Definition of initial and final states for the thermodynamic free energy model.

The change in interfacial areas for this scenario where a wetted sublayer has already formed on the surface covering the entire hydrophilic region can be expressed by modifying the Wenzel area equations from Section 3.2:

$$\Delta A_{LV,amph} = 2\pi Rh - 4\pi R_{initial}^2 - (1-f)\pi a^2 \tag{24}$$

$$\Delta A_{LS,amph} = f\pi a^2 + n_{wires} \cdot 2\pi r_{wire} \cdot l_{wire} \tag{25}$$

$$\Delta A_{SV,amph} = -\Delta A_{LS,amph} \tag{26}$$

While intuition can be used to predict the impact of geometry on chemically homogeneous surfaces that wet according to the classical Wenzel and Cassie-Baxter equations, these relationships are less clear on an amphiphilic surface. The free energy model can instead be used to predict what area fraction f is required to wet the amphiphilic surface with high contact angle droplets. Figure 14 shows the normalized free energy *vs.* contact angle for surfaces with different pore radii and area fractions. For all cases the hydrophobic tips of the nanowire features are 150 nm long and the inter-pore spacing is the same as the previous analysis (d_{pore} = 145 nm).

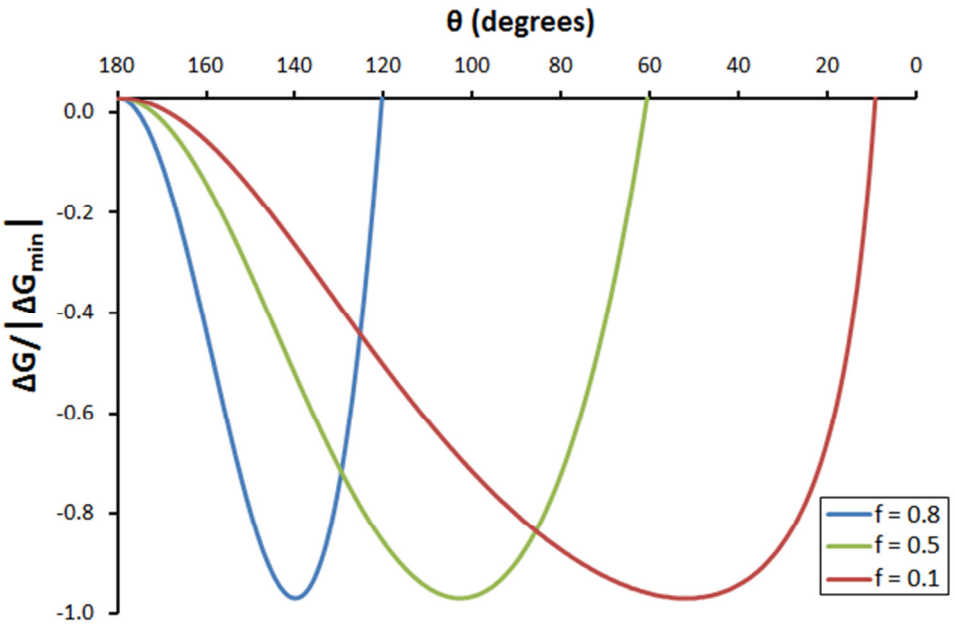

Figure 14: Free energy vs. contact angle predictions for amphiphilic surface consisting of hydrophilic base and hydrophobic tips with various area fractions, *f*. Free energy is normalized in each case by the minimum energy to show all curves on one plot.

It can be concluded from Figure 14 that much higher values of *f* are desired to produce high contact angle droplets on the amphiphilic surface as opposed those required on a chemically homogeneous surface. Uniformly hydrophobic surfaces typically have a low area fractions ranging from 0.1-0.2, as is the case in the Lau study, yet this area fraction on the amphiphilic surface with a wetted sublayer would correspond to a contact angle of roughly 50°. According to the free energy model, a much higher area fraction of 0.8 would be appropriate to produce high contact angle droplets on the amphiphilic nanostructured surface.

A high packing fraction of wires on the amphiphilic surface is desirable for condensation applications because it can (assuming the surface is made of a high thermal conductivity material) have a much higher composite thermal conductivity than surfaces

with low values of f. For this to be useful, however, the surface must also effectively manage condensate on top of the wires, i.e., the nucleated droplet growth, coalescence, and ultimately removal, a topic that is experimentally investigated in Chapter 4.

3.5 Summary

This chapter has developed and validated a thermodynamic model that not only can predict the equilibrium contact angle for the Wenzel and Cassie-Baxter states, but also can quantify which state is energetically preferred. The free energy model is then applied to surfaces which are not chemically homogeneous and therefore cannot be analyzed using the classical Wenzel and Cassie-Baxter equations. The model is an informative design tool for surfaces with local energy gradients to assess the tradeoff between control over nucleation location and reduction in the apparent contact angle.

Although the thermodynamic model does provide significant additional information, as alluded to in Figure 10, the model cannot predict local contact line phenomenon that is responsible for contact angle hysteresis and advancing/receding contact angles. This behavior is critical to condensate management; therefore, while the model is a useful starting point for designing surfaces, experiments are necessary to further understand the wetting behavior and develop more efficient condensation surfaces. The experimental investigation of the amphiphilic nanostructured surface consisting of a hydrophilic base region with hydrophobic tips first proposed in Figure 13 is the subject of Chapter 4.

CHAPTER 4

EXPERIMENTAL INVESTIGATION OF CONDENSATION ON AN AMPHIPHILIC NANOSTRUCTURED SURFACE

Having developed a model in Chapter 3 to better understand why superhydrophobic surfaces are often rendered ineffective in condensation applications and utilized this model to preliminarily assess alternative amphiphilic surfaces that could have beneficial condensation properties, this chapter focuses on experimental characterization to gain further insight that cannot be obtained *via* thermodynamic modeling. The amphiphilic surface consisting of a densely packed nanowire array made of hydrophilic base material with hydrophobic tips, introduced in Section 3.4, is fabricated and tested using both environmental scanning electron microscopy (ESEM) and high speed optical (light) visualization.

Remarkably, in addition to having a higher composite thermal conductivity in the across-the-layer direction due to its high packing fraction and presence of the liquid sub-layer, the amphiphilic nanowire surface also demonstrates the ability to produce long-range, non-contact coalescence events within a heterogeneously-sized droplet ensemble. These events thereby periodically regenerate nucleation sites without requiring condensed droplets to remain stable in the mobile Cassie state! A new mechanism is proposed for this long-range coalescence behavior involving Laplace pressure imbalance between adjacent fluidically linked droplets. The long range coalescence events create conditions favorable for heat/mass transfer by repeatedly open up fresh nucleation sites,

thereby rejuvenating the surface and generating a favorable distribution of smaller droplets.

4.1 Amphiphilic Nanostructured Surface Fabrication

The nanowire array, depicted in Figure 13, is fabricated by electrodepositing gold into a porous alumina template with 200 nm diameter pores (Whatman, Anodisc) and then selective removal of the alumina. To accomplish this, first a 50 nm layer of gold is sputtered on the branched side of the template to serve as a working electrode. Next, gold is deposited into the template using Orotemp 24 plating solution (Technic Inc.) at a potential of -0.9 V *vs.* reference electrode in a three electrode cell (consisting of a the gold working electrode, a platinum foil counter electrode and a saturated calomel reference electrode). The length of the wires is controlled by the deposition time; typically a one hour deposition yields 350 nm long wires. After deposition, the alumina template surrounding the wires is dissolved using and aqueous 3M sodium hydroxide solution. Following removal of the alumina template, the sample is extensively rinsed with nanopure (18.2 MΩ-cm resistivity) water and then freeze dried to prevent aggregation due to capillary forces during evaporation.

The process described above creates a close-packed array of 200 nm diameter hydrophilic gold wires, shown in Figure 15. The array is then made amphiphilic coating the array from the top with a hydrophobic fluoropolymer using plasma enhanced chemical vapor deposition (PECVD) [46]. Because PECVD is a directional process, the fluoropolymer only coats the tips of the nanowires, creating a surface energy gradient of low energy hydrophobic coating on the nanowire tips and native hydrophilic gold at the base. The PECVD process utilizes a flowing capacitively-coupled system operated at a

radio frequency of 13.56 MHz and power of 30W. The monomer octafluorocyclobutane (C_4F_8) is supplied to the deposition chamber at a rate of 3 scmm, along with 50 scmm of Argon gas. The chamber is held at 80 mTorr and room temperature during deposition, with the monomer inlet in the downstream position 3 inches above the substrate. The fluoropolymer is deposited for 60 seconds, leading to an approximately 10 nm thick coating on only the nanowire tips.

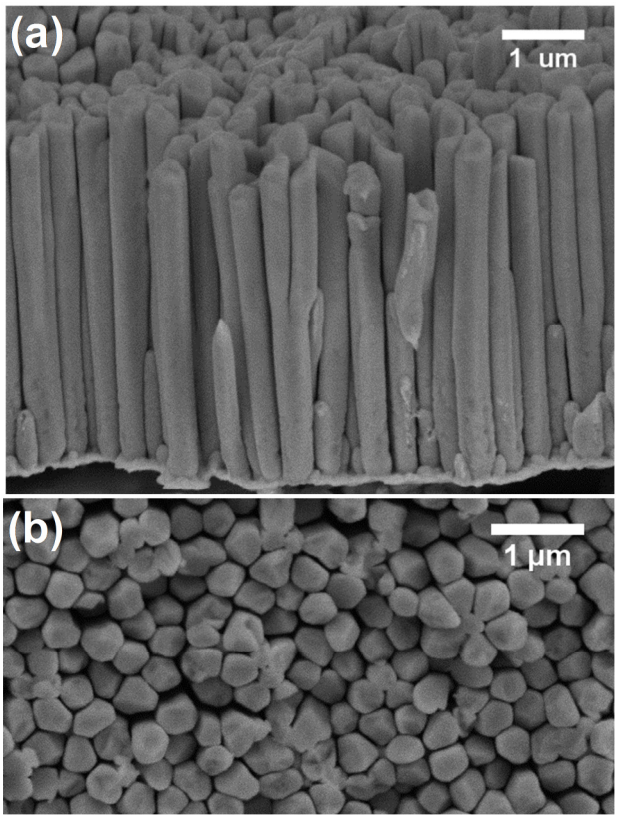

Figure 15: SEM micrographs of nanostructured surface morphology

The array is closely packed with an estimated packing fraction of 85% and less than 25 nm separating adjacent wires, determined using ImageJ analysis software (NIH). The wires are also not uniform in height, creating a secondary roughness scale and

allowing the droplets that do rest on its roughness features to only contact the tallest asperities. As a result when droplets are in the Cassie-Baxter state, they display a high contact angle because they have a minimal amount of solid-liquid contact area. This secondary roughness scale is critical to the condensation performance of this sample, as will be discussed later in the chapter.

4.2 ESEM Condensation Experiments

Environmental Scanning Electron Microscopy (ESEM) imaging is employed to investigate *in situ* condensation on the amphiphilic surface, taking advantage of the superior sub-micron spatial resolution and depth of view, as compared to optical microscopy, offered by this technique [47, 48]. The ESEM setup consists of a Peltier stage, capable of generating a maximum ΔT of 68°C and maximum cooling of 3.5W, (C2-08-0401; Tellurex, Traverse City, MI) attached to a copper heat sink to provide uniform subcooling from beneath the nanowire array sample surface. Condensation imaging is performed in a pure water vapor environment by reducing the sample surface below the water saturation temperature corresponding to a chamber pressure of 5.8 torr.

To investigate how the surface wets in the hydrophilic base region, depicted in Figure 13a, an uncoated sample is prepared without the freeze-drying step to prevent wire aggregation. The resulting nanowire array has micrometer-sized valleys which provide line-of-sight view into the area between adjacent wires. Figure 16 contains a sequence of images, proceeding left to right, illustrating the wetting behavior within the hydrophilic region. Condensation first occurs at the base of the surface, where the subcooling is greatest due to the Peltier cooler. The subsequent images shows the liquid level rising uniformly between the wire array, as indicated by the fact that the shortest wires begin to

become covered up by the rising sublayer while the longest remain visible above the liquid.

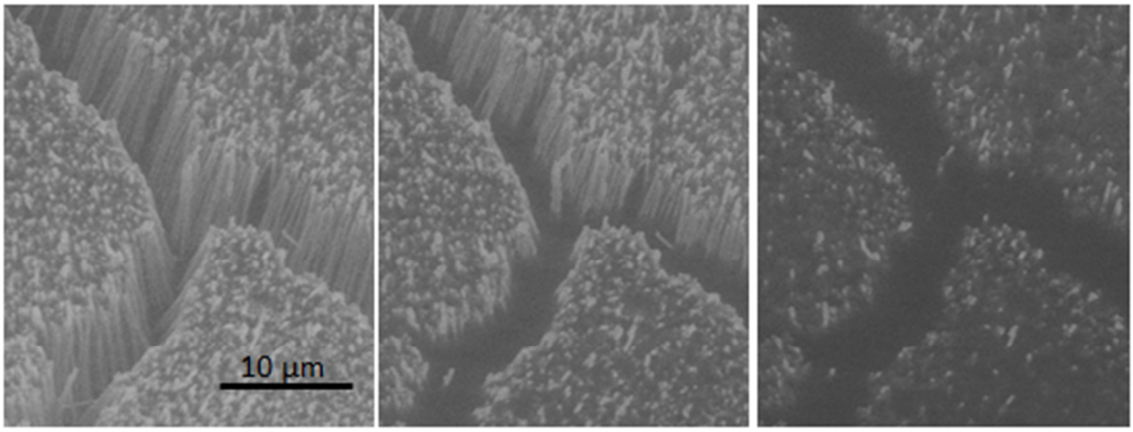

Figure 16: Development of wetted sublayer on a uniformly hydrophilic nanowire array. The surface is subcooled from beneath and the images proceed left to right, showing the liquid layer rising between the nanowires.

Having gained better insight into the wetting behavior within the hydrophilic base region, similar experiments are performed on a nanowire array that has been fluoropolymer coated and freeze dried. Imaging is performed orthogonal to the wire orientation to determine the height of the wetted sublayer relative to the wire length on the as-prepared sample. The wetted sublayer covers approximately the bottom 90% of the wire length, indicating that the hydrophobic fluoropolymer only coated to the top 10% due to the shadowing effect of the closely spaced adjacent wires shown in Figure 15. Figure 17 shows the sequence of ESEM images capturing development of the wetted sublayer and the remaining hydrophobic portion on the wire tips.

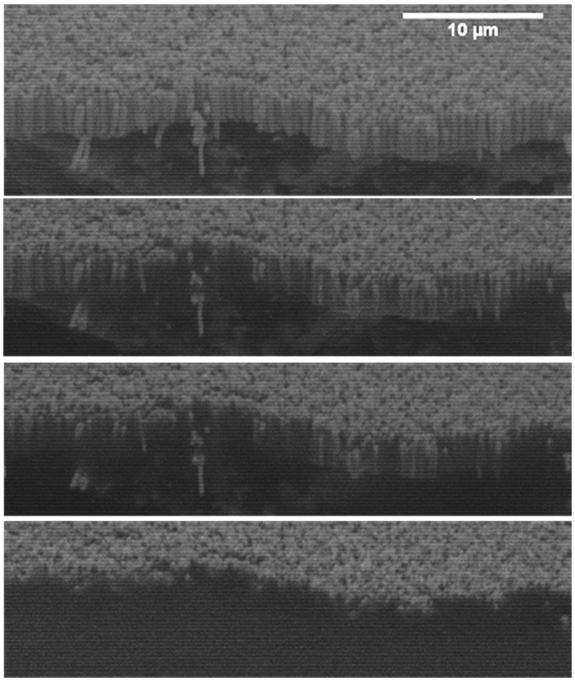

Figure 17: Sequential ESEM images showing development of the wetted sublayer and the length of the unwetted region, showing the depth of the hydrophobic fluoropolymer coating.

In addition to helping understand wetting behavior of the sublayer, *in situ* ESEM visualization is also used to investigate the dynamics of droplets that form on top of the nanowire array after development of the wetted sublayer. Sequential ESEM images, shown in Figure 18, capture droplets coalescing with neighbors and numerous smaller droplets nucleating in the space left behind.

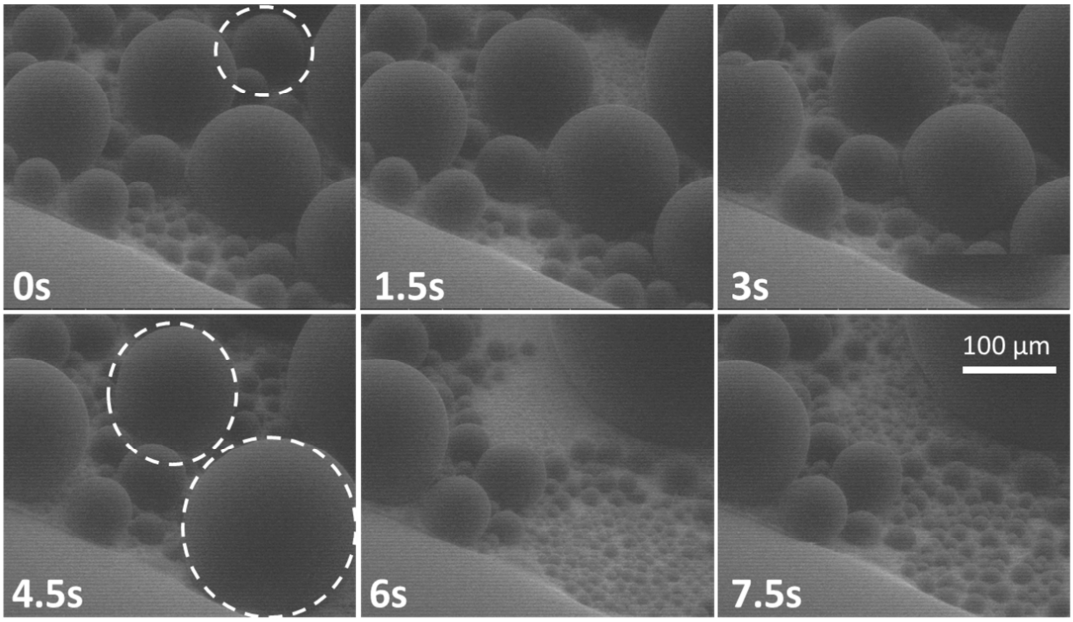

Figure 18: ESEM image sequence of coalescing droplets. Large encircled droplets coalesce with neighbors and then multiple new droplets nucleate in their wake; limited temporal resolution prevents identification of exactly which drops coalesce.

ESEM imaging offers superior spatial resolution, however the field of view is restricted by the pressure limiting aperture and the temporal resolution is limited by the scan rate required for quality imaging. Because of the 1.5 second delay between images, it is not possible to conclusively determine where the encircled droplets in Figure 18 go in the subsequent frame. As such, subsequent experiments utilizing optical microscopy are also carried out to complement the physical insight gained by the ESEM experiments.

4.3 Long-range Coalescences and Droplet Size Distribution

To gain better temporal resolution and a wider field of view, optical visualization with a Phantom v12 camera (50x objective lens) is used to compare the temporal evolution of the condensed droplet size distribution on the amphiphilic nanostructured surface to the distribution on a smooth hydrophobic surface. Ambient temperature is held

within +/- 0.5°C and relative humidity within +/- 2.5%, and to ensure consistent sub-cooling between tests DC power to a Peltier stage beneath the sample is controlled manually to cool the surface 4°C below saturation temperature for the corresponding ambient conditions. The experimental setup for optical visualization is illustrated in Figure 19.

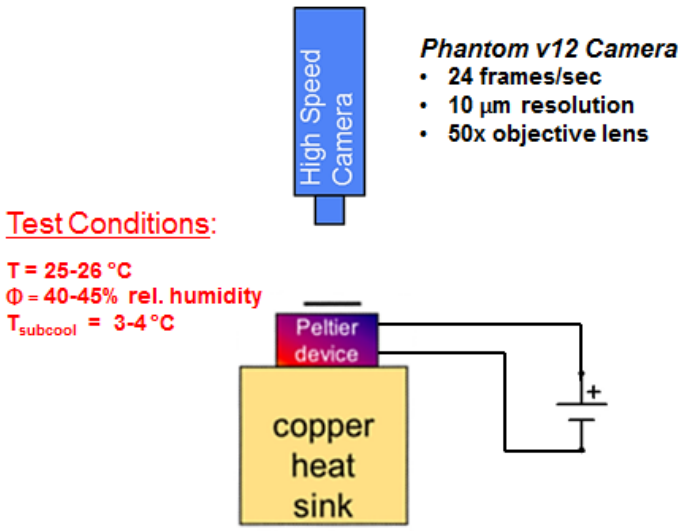

Figure 19: Experimental setup for optical visualization

Representative images at various times past the onset of condensation are shown in Figure 20. During the initial transient growth stage, both the smooth hydrophobic and the amphiphilic nanostructured surfaces exhibit similar condensation behavior. After the 3rd minute of condensation, different size droplets begin to form on the amphiphilic surface and coalescences simultaneously involving many droplets which are not in direct contact above the surface are observed. As new droplets nucleate in the space cleared behind coalesced droplets, the process repeats itself in a periodic manner. In contrast, the

droplets on the smooth hydrophobic surface grow by combination of additional vapor condensing on existing droplets and via traditional (direct contact) coalescences [49] in which adjacent droplets physically grow into one another. As a result, during 15 minutes of condensation the mean droplet size on the smooth hydrophobic surface grows to over 100 μm while on the amphiphilic surface only reaches approximately 20 μm.

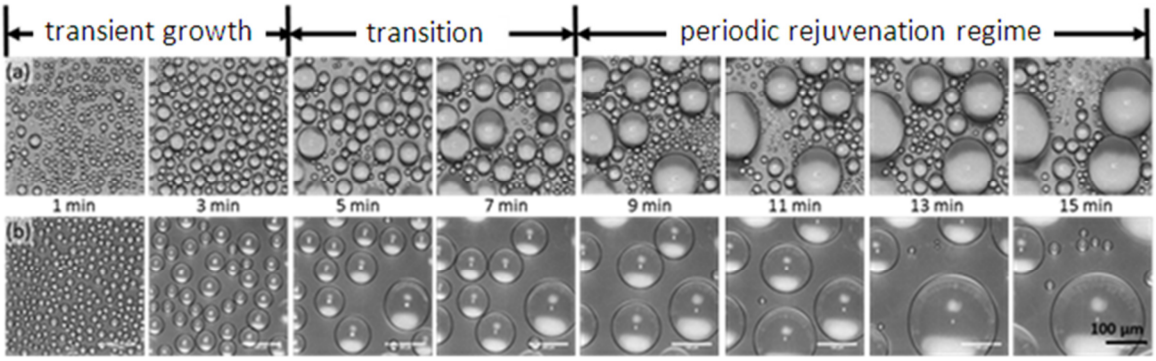

Figure 20: Temporal evolution of droplet size distribution during condensation on (a) amphiphilic nanostructured and (b) smooth hydrophobic surface

Multi-droplet non-contact based coalescences are a key aspect of the performance of the amphiphilic surface. Three examples of these long-range coalescence events involving over 10 droplets are shown in Figure 21. Red color has been added to highlight the involved droplets before (left) and after (right) the coalescence event.

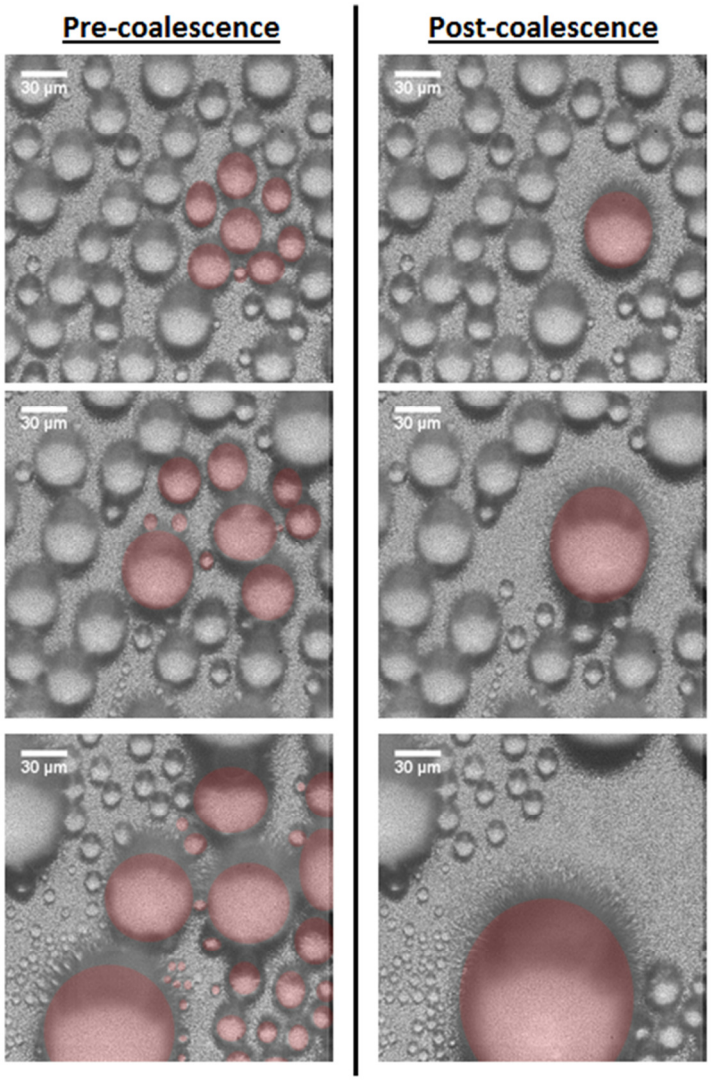

Figure 21: Long-range multi-droplet coalescence events. Multiple droplets (highlighted in red) in the images on the left coalesce simultaneously to form a single large droplet in the images on the right.

Figure 22 presents statistical information on the periodic nature of condensation on the amphiphilic surface by looking at evolution of the droplet distribution for two consecutive cycles in the periodic rejuvenation regime. The first stage of this periodic behavior, a large spike in the number of small droplets, occurs immediately following a major coalescence event as new droplets nucleate in the space left open behind the smaller droplets. This initial stage can be seen in the droplet distributions at 8 and 11

minutes past the onset of condensation. In the next stage, visible respectively at 9 and 12 minutes, the tall peak of smaller droplets in the distribution begins to flatten out and shift to the right (*i.e.*, towards few but larger droplets), as the smaller droplets coalesce with their nearest neighbors. In this second stage only 2-3 droplets coalesce at once in the traditional direct-contact induced manner, as indicated by the fact that the overall droplet count still remains relatively high. Lastly, long-range multi-droplet collective coalescence events take place during the third stage, causing the droplet distributions at 10 and 13 minutes to flatten out with significant reduction in the small droplet count, thus creating fresh nucleation sites. The surface is able to "self-rejuvenate" in this manner, and because prior studies have shown that droplets with diameters less than 10 μm contribute the most to heat transfer during dropwise condensation [7, 8], this behavior is expected to enhance heat transfer by continually nucleating new micrometer-sized droplets on a high thermal conductivity nanostructure filled with a liquid sublayer.

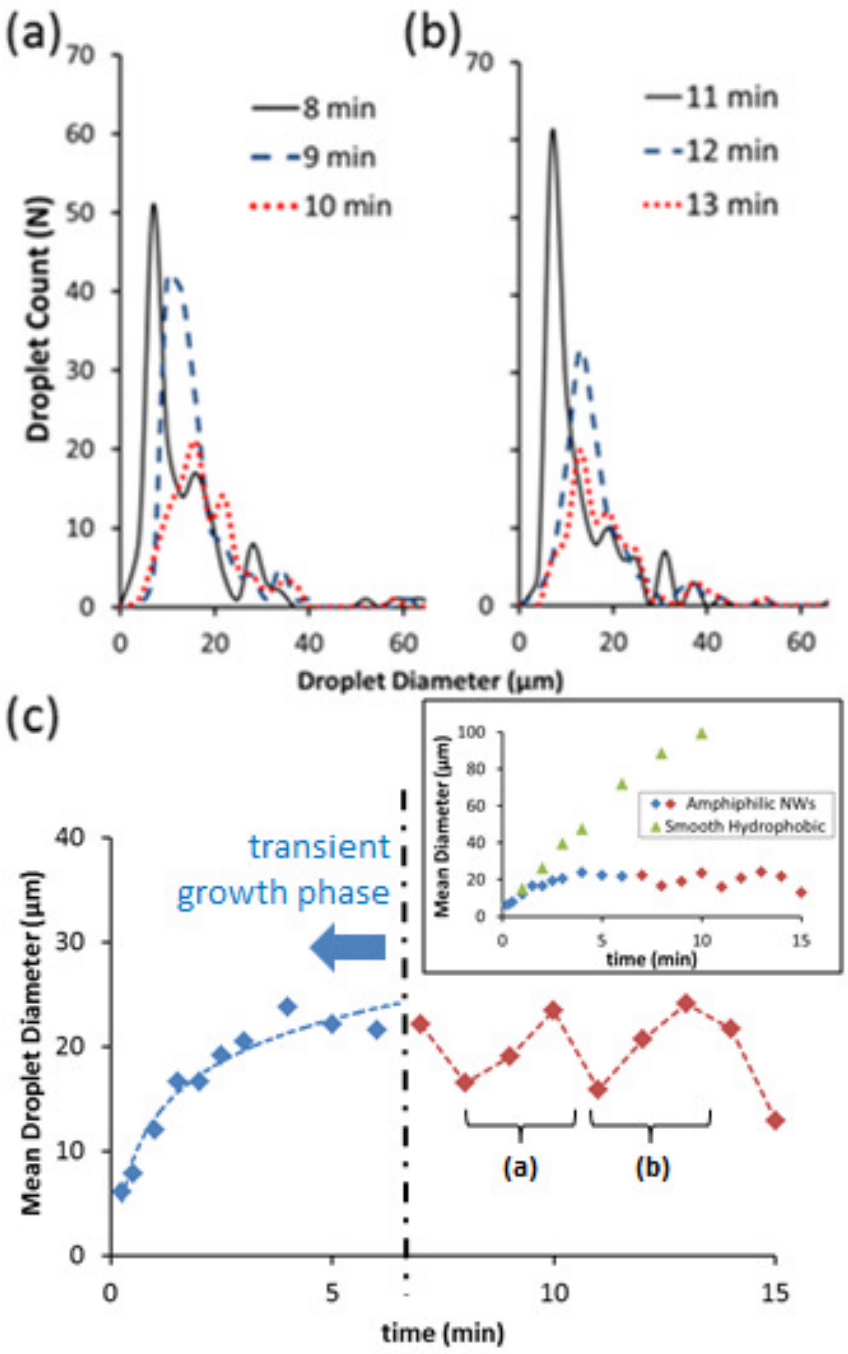

Figure 22: Droplet size distributions in the 0-60 um range at (a) 8, 9 and 10 min and (b) 11, 12 and 13 min past the onset of condensation. (c) Time history of mean droplet diameter on the amphiphilic surface.

4.4 Proposed Mechanism of Droplet Growth and Coalescence

The experimental observations from ESEM and optical visualization suggest a mechanism for droplet growth and coalescence on the amphiphilic nanostructured surface. The sequence of ESEM images in Figure 23 illustrate the process of droplets emerging from the nanowire array. Upon initial cooling below saturation temperature, a layer of condensate forms at the base of the wires (Fig. 23a-b) due to preferential nucleation and capillary condensation on the hydrophilic surface.

Once the hydrophilic portion is fully wetted, droplets nucleate on the hydrophobic wire tips. These droplets are initially in the Cassie state, as indicated by the fact that they are highly spherical and exhibit contact angles greater than 150 (Fig. 23c-d). The intrinsic contact angle, θ_y, is roughly 108° for a fluoropolymer on a smooth surface [50], meaning that in order to have a macroscopic contact angle of over 150° the area underneath the droplet base that contacts solid must be less than 20% of the total droplet base area according to the Cassie-Baxter equation from Chapter 2. This observation highlights the importance of the secondary roughness caused by the difference in wire heights, because with a wire packing fraction of approximately 85%, the initial Cassie droplets must only contact a fraction of the (tallest) wires beneath it to achieve a 20% area fraction. Further, roughness features must truly be nano-sized to support droplets with diameters on the order of 10 μm, because a high number of wires at different heights must be present beneath this small droplet for the above described behavior to occur.

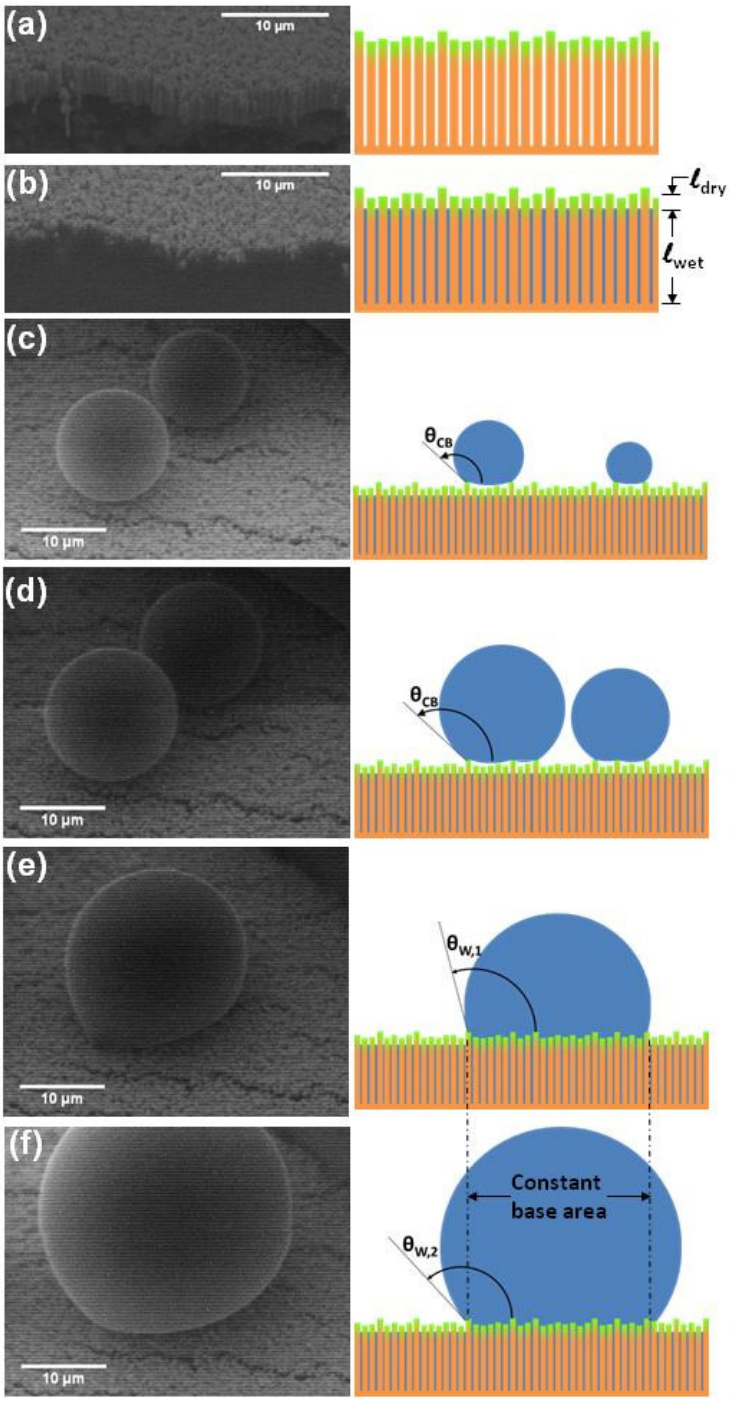

Figure 23: ESEM images of condensation wetting stages. (a) Dry amphiphilic surface. (b) Subcooling leads to nucleation at base. (c) Formation and (d) constant contact angle growth of Cassie droplets. (e) Contact-based coalescence of Cassie drops. (f) Growth of resulting Wenzel drop with a constant base area.

Eventually adjacent droplets in the Cassie-Baxter state coalesce by growing into one another, and in doing so transition to the Wenzel state wherein they are connected to the underlying fluid layer. This transition can be seen by a post-coalescence reduction in contact angle, and by the fact that a coalesced droplet grows in a constant base area mode with a high degree of contact line pinning, behavior that is characteristic of the Wenzel state.

The insight gained from ESEM visualization of the wetted sublayer development and initial droplet dynamics offers a more complete understanding of the phenomenon occurring in the quasi-periodic steady state regime depicted in Figures 20 and 22. After undergoing at least one coalescence, droplets transition to a Wenzel state and are thus fluidically linked *via* the wetted sublayer between the hydrophilic portions of the nanowires. In the steady state regime, there is an assortment of Wenzel state droplets of varying diameter within close proximity of one another. Thermodynamically, droplets on a surface will always prefer to coalesce into one larger droplet to minimize the total surface free energy, however on a typical hydrophobic surface there is no path to this lower energy state. In contrast, on the amphiphilic surface the Laplace pressure difference between adjacent droplets with different radii of curvature supplies the driving force for coalescence and the fluidic linkage through the sublayer provides the pathway. A representative coalescence sequence with an illustrated schematic is highlighted in Figure 24. It is clear that the droplets do coalesce into one, rather than moving radially outward from the field of view, because a region of droplets fully surrounding each coalescence zone remains unaffected during the event. Furthermore the fact that two small droplets, presumably in the Cassie state due to their small size, are unaffected by the coalescence

of the surrounding droplets provides strong evidence supporting the proposed mechanism of non-direct contact coalescence through the wetted sublayer. If the larger Wenzel droplets were instead coalesced above the surface by a cascade of adjacent contacting droplets these Cassie droplets would undoubtedly be swept up in the process. It is important to note, however, that both contact-based and Laplace pressure-driven coalescences can occur simultaneously, as indicated in Figure 24 by the other small Cassie droplets which are within the footprint of the final coalesced drop and therefore do participate in the coalescence.

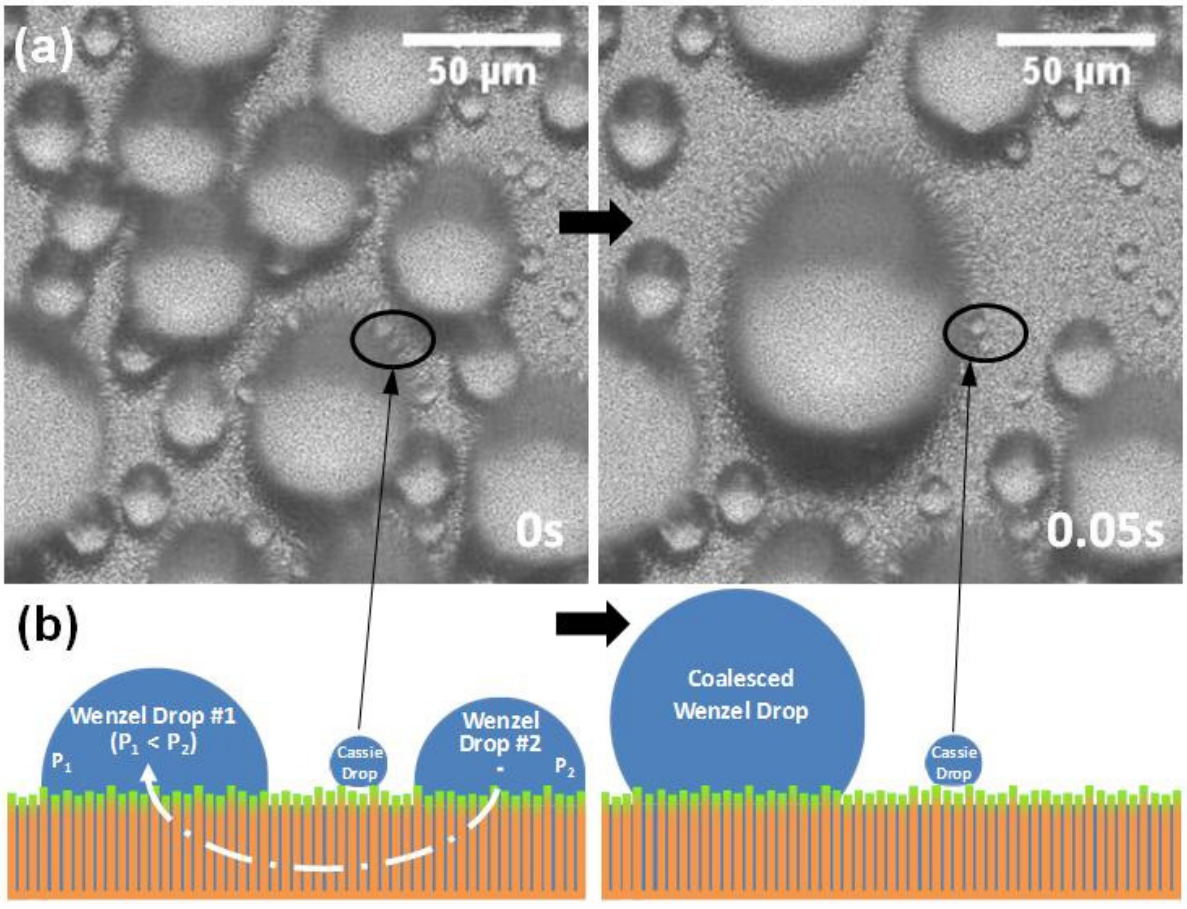

Figure 24: (a) Pre- and post-coalescence optical images of a Laplace pressure driven multi-droplet long range coalescence event. (b) Sketched schematic of the coalescence process.

4.5 Summary

A novel nanostructured amphiphilic surface, consisting of hydrophilic base and hydrophobic tops of high density nanowire array, is fabricated and experimentally investigated in this chapter. The results of condensation experiments demonstrate that such a surface enables long-range collective coalescence events – a new phenomenon resulting in periodic generation of fresh nucleation sites for small droplets during dropwise condensation. ESEM and optical visualization suggest that this regenerative behavior is achieved by Laplace-pressure driven coalescence of Wenzel droplets through the wetted sublayer, rather than requiring condensed droplets to remain stable in the Cassie state such that they can roll off the surface. This type of amphiphilic surface is promising for condensation applications because of its high thermal conductivity along with dropwise mode of condensation and has fabrication advantageous in that the roughness is generated in a single step, rather than requiring fabrication of microscale roughness followed by subsequent growth of nanostructures as utilized in other studies [19-25].

The issue of removing the few large "sticky" Wenzel droplets remains even for these new amphiphilic surfaces, which needs to be addressed for practical applications of designing heat transfer equipment. However, the fact that the wetted sublayer provides a path for droplet coalescence from a longer range means that the largest droplets can more rapidly collect volume and grow to a size where removal becomes practical. For example, on a vertically oriented surface eventually gravitational forces will become significant relative to surface forces at which point the largest droplets can slide off the surface.

Regardless of removal mechanism, during the time in which the largest droplets grow to a size practical for removal, a heat transfer enhancement is expected in the area of the surface immediately surrounding these droplets as moderately sized Wenzel droplets are drawn in by the Laplace pressure imbalance and fresh nucleation sites are created in their wake. With further exploration and optimization, this type of amphiphilic surface could provide an alternative mode of dropwise condensation to that of traditional superhydrophobic surfaces, thus opening new avenues for a broad range of critical moisture and thermal management applications in emerging thermally limited nanotechnologies.

CHAPTER 5

CONCLUSIONS AND FUTURE WORK

Condensation is an important phenomenon for both established industries, such as water management in paper manufacturing and steam power plants, and emerging technologies, including thermal management of high performance microprocessors and high energy density batteries which require ultra-efficient heat removal. Effective management of the condensed liquid is critical in maximizing condensation heat and mass transfer rates. Traditional superhydrophobic surfaces have recently been investigated to enhance removal of condensed water; however, designing superhydrophobic surfaces which are robust to condensation has proven problematic. Even surfaces which do retain their superhydrophobicity during condensation suffer from other disadvantages, including limited thermal contact area between the droplet and substrate and high free energy barrier for nucleation. To better understand these limitations and investigate alternative solutions, this work focused in two main areas.

First, a thermodynamic free energy based model was developed to explain why traditional superhydrophobic surfaces often lose their superhydrophobic properties during condensation. It was found that while the Cassie-Baxter state is a local free energy minimum for a large droplet placed on a substrate, the Wenzel state is often the global energy minimum, and condensate droplets that nucleate on a length scale smaller than the surface roughness features will access this global minimum energy state and remain pinned to the surface. The free energy model was validated in two ways, first by ensuring predicted contact angles for each state match the traditional Wenzel and Cassie-Baxter

model, and secondly by comparing the critical nanowire length which resulted in an experimentally observed transition from the Wenzel to Cassie-Baxter wetting state [19]. Once validated, the model was extended to evaluate different nanostructure geometries and expanded to analyze the effect of spatial non-homogeneity scenarios where varying regions of the surface have different surface energies. Based on the thermodynamic calculations, a promising alternative surface structure was identified, consisting of densely packed amphiphilic nanowire arrays with hydrophilic base region and hydrophobic tips.

The second major component of this work consisted of fabricating the proposed amphiphilic nanostructured arrays and experimentally assessing their condensation performance. Complementary ESEM and optical microscopy were utilized to show that droplets on the amphiphilic interface are fluidically linked by a wetted sublayer that fills the hydrophilic region on the surface. This fluidic sublayer allows neighboring droplets to coalesce more rapidly and simultaneously in large ensembles. A mechanism involving Laplace pressure-driven flow through the wetted sublayer was proposed based on the experimental observations.

Numerous new avenues of research could result from this initial investigation into the use of amphiphilic nanostructured surfaces for enhanced condensation heat and mass transfer. On the fundamental front, of particular interest would be even the higher speed visualization, which may provide further insight into the physics of the observed coalescence phenomenon, potentially capturing the local details of rapid transient interactions between droplets and the substrate. On practical side, it is also important to note that while the amphiphilic surface results in rapid regeneration of nucleation sites, to

become viable for industrial applications it is important to identify a method to remove the largest droplets that are formed as a result of the rapid coalescences. If placed on a vertical substrate, the droplets will eventually grow large enough to be removed by gravity, however alternate techniques such as vibration induced dewetting [51], may be employed to remove the largest droplets at a greater frequency. Lastly, development of new amphiphilic surface geometries, which are effective in droplet nucleation, growth and autonomous (passive) condensate removal as well as scalable over large areas, manufacturable and robust when used in often aggressive environments found in condensation applications, is an important dimension for future work in this field.

APPENDIX A

EES FREE ENERGY MODEL

```
R_i=50e-6[m]
V_droplet=(4*pi)/3*R_i^3
d_pore=145e-9 [m]
r_wire=25e-9 [m]
l_wire=200e-9 [m]
AR=l_wire/(r_wire*2)
"
Interfacial Energy Parameters:"
gamma_LV=72.9e-3 [J/m^2]
gamma_SV=18.0e-3 [J/m^2]
theta_young=108[degrees]
gamma_SV=gamma_LV*cos(theta_young)+gamma_LS
"
Cassie & Wenzel Equations:"
roughness=1+((4*pi)/SQRT(3))*(r_wire*l_wire)/((d_pore)^2)
f=(2*pi)/(SQRT(3))*(r_wire/d_pore)^2
cos(theta_W)=IF(roughness*cos(theta_young),-1,-1,-1,roughness*cos(theta_young))
cos(theta_CB)=f*cos(theta_young)+f-1
"
Gibbs Energy vs. Macroscopic Contact Angle Analysis:"
duplicate j=0,180
        theta[j]=180-j/2
"
Wenzel Wetting Analysis:"
        a[j]=R[j]*sin(theta[j])
        h[j]=R[j]*(1-cos(theta[j]))
        n_wires[j]=f*(a[j]/r_wire)^2
        V_droplet=((pi*h[j])/6)*(3*a[j]^2+h[j]^2)
        DELTAA_LV_W[j]=2*pi*R[j]*h[j]-4*pi*R_i^2
        DELTAA_LS_W[j]=pi*a[j]^2+n_wires[j]*2*pi*r_wire*l_wire
        DELTAG_W[j]=gamma_LV*DELTAA_LV_W[j]+(gamma_LS-
gamma_SV)*DELTAA_LS_W[j]
"
Cassie-Baxter Wetting Analysis:"
        DELTAA_LV_CB[j]=2*pi*R[j]*h[j]+pi*a[j]^2*(1-f)-4*pi*R_i^2
        DELTAA_LS_CB[j]=pi*a[j]^2*f
        DELTAG_CB[j]=gamma_LV*DELTAA_LV_CB[j]+(gamma_LS-
gamma_SV)*DELTAA_LS_CB[j]
end
```

cos(theta_young)=(f-1)/(roughness_critical-f)
roughness_critical=1+((4*pi)/SQRT(3))*(r_wire*l_wire_critical)/((d_pore)^2)
AR_critical=l_wire_critical/(r_wire*2)

REFERENCES

[1] P. G. Degennes, "WETTING - STATICS AND DYNAMICS," *Reviews of Modern Physics,* vol. 57, pp. 827-863, 1985.

[2] S. H. Kim, "Fabrication of superhydrophobic surfaces," *Journal of Adhesion Science and Technology,* vol. 22, pp. 235-250, 2008.

[3] M. Nosonovsky and B. Bhushan, "Superhydrophobic surfaces and emerging applications: Non-adhesion, energy, green engineering," *Current Opinion in Colloid & Interface Science,* vol. 14, pp. 270-280, 2009.

[4] C. R. Crick and I. P. Parkin, "Preparation and Characterisation of Super-Hydrophobic Surfaces," *Chemistry-a European Journal,* vol. 16, pp. 3568-3588, 2010.

[5] M. Nosonovsky and B. Bhushan, "Biomimetic superhydrophobic surfaces: Multiscale approach," *Nano Letters,* vol. 7, pp. 2633-2637, 2007.

[6] K. Rykaczewski and J. H. J. Scott, "Methodology for Imaging Nano-to-Microscale Water Condensation Dynamics on Complex Nanostructures," vol. 5, pp. 5962-5968, 2011.

[7] C. Graham and P. Griffith, "Drop Size Distributions and Heat-Transfer in Dropwise Condensation," *International Journal of Heat and Mass Transfer,* vol. 16, pp. 337-346, 1973.

[8] J. W. Rose and L. R. Glicksman, "Dropwise Condensation - Distribution of Drop Sizes," *International Journal of Heat and Mass Transfer,* vol. 16, pp. 411-425, 1973.

[9] E. Schmidt, W. Schurig, and W. Sellschopp, "Condensation of water vapour in film- and drop form," *Zeitschrift Des Vereines Deutscher Ingenieure,* vol. 74, pp. 544-544, 1930.

[10] J. W. Rose, "Dropwise condensation theory and experiment: a review," *Proceedings of the Institution of Mechanical Engineers Part a-Journal of Power and Energy,* vol. 216, pp. 115-128, 2002.

[11] V. P. Carey, *Liquid-vapor phase-change phenomena : an introduction to the thermophysics of vaporization and condensation processes in heat transfer equipment*. Washington, D.C. Hemisphere Pub. Corp., 1992.

[12] D. Beysens and C. M. Knobler, "GROWTH OF BREATH FIGURES," *Physical Review Letters,* vol. 57, pp. 1433-1436, 1986.

[13] A. Steyer, P. Guenoun, D. Beysens, and C. M. Knobler, "GROWTH OF DROPLETS ON A SUBSTRATE BY DIFFUSION AND COALESCENCE," *Physical Review A,* vol. 44, pp. 8271-8277, 1991.

[14] P. Meakin and F. Family, "SCALING IN THE KINETICS OF DROPLET GROWTH AND COALESCENCE - HETEROGENEOUS NUCLEATION," *Journal of Physics A,* vol. 22, pp. L225-L230, 1989.

[15] P. Meakin, "DIFFUSION-LIMITED DROPLET COALESCENCE," *Physica A,* vol. 165, pp. 1-18, 1990.

[16] D. Beysens, "Dew nucleation and growth," *Comptes Rendus Physique,* vol. 7, pp. 1082-1100, 2006.

[17] C. Dorrer and J. Ruhe, "Some thoughts on superhydrophobic wetting," *Soft Matter,* vol. 5, pp. 51-61, 2009.
[18] D. Quere, "Non-sticking drops," *Reports on Progress in Physics,* vol. 68, pp. 2495-2532, 2005.
[19] K. K. S. Lau, J. Bico, K. B. K. Teo, M. Chhowalla, G. A. J. Amaratunga, W. I. Milne*, et al.*, "Superhydrophobic Carbon Nanotube Forests," *Nano Letters,* vol. 3, pp. 1701-1705, 2003.
[20] C. H. Chen, Q. J. Cai, C. L. Tsai, C. L. Chen, G. Y. Xiong, Y. Yu*, et al.*, "Dropwise condensation on superhydrophobic surfaces with two-tier roughness," *Applied Physics Letters,* vol. 90, 2007.
[21] J. B. Boreyko and C. H. Chen, "Self-Propelled Dropwise Condensate on Superhydrophobic Surfaces," *Physical Review Letters,* vol. 103, 2009.
[22] X. Chen, J. Wu, R. Ma, M. Hua, N. Koratkar, S. Yao*, et al.*, "Nanograssed Micropyramidal Architectures for Continuous Dropwise Condensation," *Advanced Functional Materials,* pp. n/a-n/a, 2011.
[23] K. K. Varanasi, M. Hsu, N. Bhate, W. S. Yang, and T. Deng, "Spatial control in the heterogeneous nucleation of water," *Applied Physics Letters,* vol. 95, 2009.
[24] C. Dietz, K. Rykaczewski, A. G. Fedorov, and Y. Joshi, "Visualization of droplet departure on a superhydrophobic surface and implications to heat transfer enhancement during dropwise condensation," *Applied Physics Letters,* vol. 97, 2010.
[25] N. A. Patankar, "Supernucleating surfaces for nucleate boiling and dropwise condensation heat transfer," *Soft Matter,* vol. 6, pp. 1613-1620, 2010.
[26] R. N. Wenzel, "Resistance of Solid Surfaces to Wetting by Water," *Industrial & Engineering Chemistry,* vol. 28, pp. 988-994, 1936.
[27] A. B. D. Cassie and S. Baxter, "Wettability of porous surfaces," *Transactions of the Faraday Society,* vol. 40, pp. 546-551, 1944.
[28] L. Gao and T. J. McCarthy, "How Wenzel and Cassie Were Wrong," *Langmuir,* vol. 23, pp. 3762-3765, 2007.
[29] L. C. Gao and T. J. McCarthy, "Reply to "Comment on How Wenzel and Cassie Were Wrong by Gao and McCarthy"," *Langmuir,* vol. 23, pp. 13243-13243, 2007.
[30] G. McHale, "Cassie and Wenzel: Were They Really So Wrong?," *Langmuir,* vol. 23, pp. 8200-8205, 2007.
[31] M. Nosonovsky, "On the range of applicability of the Wenzel and Cassie equations," *Langmuir,* vol. 23, pp. 9919-9920, 2007.
[32] M. V. Panchagnula and S. Vedantam, "Comment on How Wenzel and Cassie Were Wrong by Gao and McCarthy," *Langmuir,* vol. 23, pp. 13242-13242, 2007.
[33] T. D. K. K. Varanasi, US Patent Application NO. 12/254561 Patent, 2008.
[34] Y. T. Cheng and D. E. Rodak, "Is the lotus leaf superhydrophobic?," *Applied Physics Letters,* vol. 86, 2005.
[35] Y. T. Cheng, D. E. Rodak, A. Angelopoulos, and T. Gacek, "Microscopic observations of condensation of water on lotus leaves," *Applied Physics Letters,* vol. 87, 2005.
[36] R. D. Narhe and D. A. Beysens, "Nucleation and growth on a superhydrophobic grooved surface," *Physical Review Letters,* vol. 93, 2004.

[37] K. A. Wier and T. J. McCarthy, "Condensation on Ultrahydrophobic Surfaces and Its Effect on Droplet Mobility: Ultrahydrophobic Surfaces Are Not Always Water Repellant," *Langmuir,* vol. 22, pp. 2433-2436, 2006.
[38] A. Lafuma and D. Quere, "Superhydrophobic states," *Nature Materials,* vol. 2, pp. 457-460, 2003.
[39] N. A. Patankar, "Transition between superhydrophobic states on rough surfaces," *Langmuir,* vol. 20, pp. 7097-7102, 2004.
[40] A. Marmur, "Wetting on hydrophobic rough surfaces: To be heterogeneous or not to be?," *Langmuir,* vol. 19, pp. 8343-8348, 2003.
[41] J. B. Boreyko, Y. Zhao, and C.-H. Chen, "Planar jumping-drop thermal diodes," *Applied Physics Letters,* vol. 99, 2011.
[42] N. Miljkovic, R. Enright, and E. N. Wang, "Effect of Droplet Morphology on Growth Dynamics and Heat Transfer during Condensation on Superhydrophobic Nanostructured Surfaces," *ACS Nano,* vol. 6, pp. 1776-1785, 2012.
[43] K. Rykaczewski, W. A. Osborn, J. Chinn, M. L. Walker, J. H. J. Scott, W. Jones*, et al.*, "How nanorough is rough enough to make a surface superhydrophobic during water condensation?," *Soft Matter,* vol. 8, pp. 8786-8794, 2012.
[44] K. Rykaczewski, "Microdroplet Growth Mechanism during Water Condensation on Superhydrophobic Surfaces," *Langmuir,* vol. 28, pp. 7720-7729, 2012.
[45] S. Daniel, M. K. Chaudhury, and J. C. Chen, "Past drop movements resulting from the phase change on a gradient surface," *Science,* vol. 291, pp. 633-636, 2001.
[46] K. D. Anderson, J. M. Slocik, M. E. McConney, J. O. Enlow, R. Jakubiak, T. J. Bunning*, et al.*, "Facile Plasma-Enhanced Deposition of Ultrathin Crosslinked Amino Acid Films for Conformal Biometallization," *Small,* vol. 5, pp. 741-749, 2009.
[47] B. Bhushan and Y. C. Jung, "Wetting behaviour during evaporation and condensation of water microdroplets on superhydrophobic patterned surfaces," *Journal of Microscopy-Oxford,* vol. 229, pp. 127-140, 2008.
[48] K. Rykaczewski, J. H. J. Scott, and A. G. Fedorov, "Electron beam heating effects during environmental scanning electron microscopy imaging of water condensation on superhydrophobic surfaces," *Applied Physics Letters,* vol. 98, 2011.
[49] W. D. Ristenpart, P. M. McCalla, R. V. Roy, and H. A. Stone, "Coalescence of spreading droplets on a wettable substrate," *Physical Review Letters,* vol. 97, p. 4, 2006.
[50] H. W. Fox and W. A. Zisman, "The spreading of liquids on low energy surfaces. I. polytetrafluoroethylene," *Journal of Colloid Science,* vol. 5, pp. 514-531, 1950.
[51] J. B. Boreyko and C. H. Chen, "Restoring Superhydrophobicity of Lotus Leaves with Vibration-Induced Dewetting," *Physical Review Letters,* vol. 103, 2009.